

See discussions, stats, and author profiles for this publication at: <https://www.researchgate.net/publication/23768509>

Design, Selection, and Characterization of Thioflavin-Based Intercalation Compounds with Metal Chelating Properties for Application in Alzheimer's Disease

ARTICLE in JOURNAL OF THE AMERICAN CHEMICAL SOCIETY · FEBRUARY 2009

Impact Factor: 12.11 · DOI: 10.1021/ja806062g · Source: PubMed

CITATIONS

118

READS

56

10 AUTHORS, INCLUDING:



[Cristina Rodriguez-Rodriguez](#)

University of British Columbia - Vancouver

18 PUBLICATIONS 313 CITATIONS

SEE PROFILE



[Salvador Ventura](#)

Autonomous University of Barcelona

161 PUBLICATIONS 3,598 CITATIONS

SEE PROFILE



[Josep Vendrell](#)

Autonomous University of Barcelona

98 PUBLICATIONS 2,342 CITATIONS

SEE PROFILE



[Mariona Sodupe](#)

Autonomous University of Barcelona

189 PUBLICATIONS 4,600 CITATIONS

SEE PROFILE

Design, Selection, and Characterization of Thioflavin-Based Intercalation Compounds with Metal Chelating Properties for Application in Alzheimer's Disease

Cristina Rodríguez-Rodríguez,[†] Natalia Sánchez de Groot,[‡] Albert Rimola,[†] Ángel Álvarez-Larena,[§] Vega Lloveras,^{||} José Vidal-Gancedo,^{||,⊥} Salvador Ventura,[‡] Josep Vendrell,[‡] Mariona Sodupe,[†] and Pilar González-Duarte^{*,†}

Departament de Química, Departament de Bioquímica i Biologia Molecular and Institut de Biotecnologia i de Biomedicina, and Servei de Difracció de Raigs X, Universitat Autònoma de Barcelona, E-08193 Bellaterra, Barcelona, Spain, and Institut de Ciència de Materials de Barcelona (CSIC) and Networking Centre on Bioengineering, Biomaterials and Nanomedicine (CIBER-BBN), Campus Universitari de Bellaterra, E-08193 Bellaterra, Barcelona, Spain

Received August 1, 2008; E-mail: pilar.gonzalez.duarte@uab.cat

Abstract: Metal chelation is considered a rational therapeutic approach for interdicting Alzheimer's amyloid pathogenesis. At present, enhancing the targeting and efficacy of metal-ion chelating agents through ligand design is a main strategy in the development of the next generation of metal chelators. Inspired by the traditional dye Thioflavin-T, we have designed new multifunctional molecules that contain both amyloid binding and metal chelating properties. In silico techniques have enabled us to identify commercial compounds that enclose the designed molecular framework (**M1**), include potential antioxidant properties, facilitate the formation of iodine-labeled derivatives, and can be permeable through the blood–brain barrier. Iodination reactions of the selected compounds, 2-(2-hydroxyphenyl)benzoxazole (**HBX**), 2-(2-hydroxyphenyl)benzothiazole (**HBT**), and 2-(2-aminophenyl)-1*H*-benzimidazole (**BM**), have led to the corresponding iodinated derivatives **HBXI**, **HBTI**, and **BMI**, which have been characterized by X-ray diffraction. The chelating properties of the latter compounds toward Cu(II) and Zn(II) have been examined in the solid phase and in solution. The acidity constants of **HBXI**, **HBTI**, and **BMI** and the formation constants of the corresponding ML and ML₂ complexes [M = Cu(II), Zn(II)] have been determined by UV–vis pH titrations. The calculated values for the overall formation constants for the ML₂ complexes indicate the suitability of the **HBXI**, **HBTI**, and **BMI** ligands for sequestering Cu(II) and Zn(II) metal ions present in freshly prepared solutions of β -amyloid (A β) peptide. This was confirmed by A β aggregation studies showing that these compounds are able to arrest the metal-promoted increase in amyloid fibril buildup. The fluorescence features of **HBX**, **HBT**, **BM**, and the corresponding iodinated derivatives, together with fluorescence microscopy studies on two types of pregrown fibrils, have shown that **HBX** and **HBT** compounds could behave as potential markers for the presence of amyloid fibrils, whereas **HBXI** and **HBTI** may be especially suitable for radioisotopic detection of A β deposits. Taken together, the results reported in this work show the potential of new multifunctional thioflavin-based chelating agents as Alzheimer's disease therapeutics.

Introduction

The devastating effects of Alzheimer's disease (AD) on human beings and its predicted increase in incidence in the coming years due to the aging of society account for the current intensive studies aimed at preventing and treating AD.^{1–4} β -Amyloid (A β) plaques, which are a key neuropathological

feature of AD, are mainly constituted by aggregation of the A β peptide, a 39- to 43-residue degradation fragment of a much larger A β precursor protein (APP). The origin of these insoluble extracellular neurotoxic deposits is still not clear, and multiple factors such as pH, metal ions, protein concentration, and oxidative stress have been reported to trigger their formation. To date, the potential anti-amyloid therapeutic approaches to AD focus on the amyloid cascade theory, the A β vaccine, or treatment with metal-complexing agents.^{1,5,6}

[†] Departament de Química, Universitat Autònoma de Barcelona.

[‡] Departament de Bioquímica i Biologia Molecular and Institut de Biotecnologia i de Biomedicina, Universitat Autònoma de Barcelona.

[§] Servei de Difracció de Raigs X, Universitat Autònoma de Barcelona.

^{||} Institut de Ciència de Materials de Barcelona (CSIC), Campus Universitari de Bellaterra.

[⊥] Networking Centre on Bioengineering, Biomaterials and Nanomedicine (CIBER-BBN), Campus Universitari de Bellaterra.

(1) Finefrock, A. E.; Bush, A. I.; Doraiswamy, P. M. *J. Am. Geriatr. Soc.* **2003**, *51*, 1143–1148.

(2) Nordberg, A. *Lancet Neurol.* **2004**, *3*, 519–527.

(3) Brown, D. R.; Kozlowski, H. *Dalton Trans.* **2004**, 1907–1917.

(4) Storr, T.; Merkel, M.; Song-Zhao, G. X.; Scott, L. E.; Green, D. E.; Bowen, M. L.; Thompson, K. H.; Patrick, B. O.; Schugar, H. J.; Orvig, C. *J. Am. Chem. Soc.* **2007**, *129*, 7453–7463.

(5) Barnham, K. J.; Bush, A. I. *Curr. Opin. Chem. Biol.* **2008**, *12*, 222–228.

(6) Barnham, K. J.; Cherny, R. A.; Cappai, R.; Melov, S.; Masters, C. L.; Bush, A. I. *Drug Des. Rev.—Online* **2004**, *1*, 75–82.

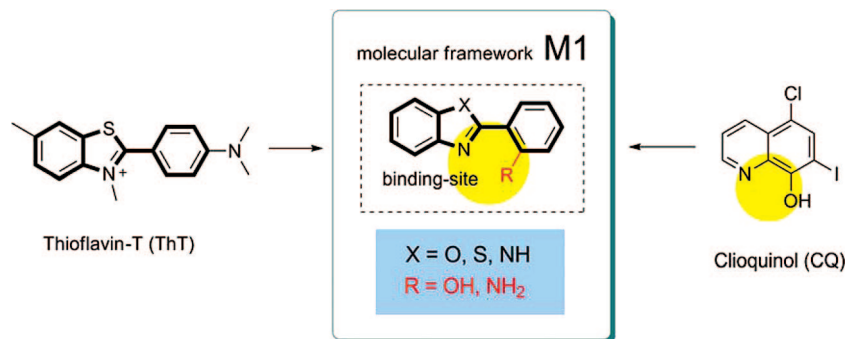


Figure 1. Combination of the main features of ThT and CQ provides a molecular framework (**M1**) with potential intercalating and chelating properties.

Aggregated $A\beta$ in senile plaques has a β -sheet secondary structure and is arranged in fibrils that exhibit specific tinctorial properties. Because of their strong affinities for fibrillar amyloid proteins, dyes such as thioflavin-T (ThT) and congo red (CR) have historically been widely used as markers to examine in vitro tissue sections for amyloid deposits.^{7–10} However, the understanding of the binding of these dyes to amyloid fibrils is still the focus of study.^{7,8} The search for ThT derivatives with higher specificities for $A\beta$ fibrils and lipophilicities adequate for crossing the blood–brain barrier (BBB) is also a field of current concern.^{11,12} These developments would enable the design of new dyes that could allow the identification of $A\beta$ fibrils from other amyloid deposits and, eventually, their use as biomarkers for the earlier detection of AD in vivo. Within the context of diagnosis, the development of small radiolabeled analogues of CR and ThT has recently led to promising in vivo imaging of amyloid in patients with AD.²

The mounting evidence supporting the role of metal ions in the pathology of AD has rendered metal-ion chelation therapy a promising treatment strategy.^{6,13–20} Among the various potential ligands reported to date, several compounds, such as desferrioxamine (DFO), DP-109, and clioquinol (CQ), an 8-hydroxyquinoline chelator, have been evaluated with relative success in transgenic mice.^{16,21,22} In addition to their metal binding abilities, chelating agents can be designed to include radical scavenger and antioxidant properties, i.e., by enclosing phenolic moieties, thus inhibiting neurotoxicity in AD.^{23,24} In fact, enhancing the targeting and efficacy of the metal-ion chelating agents through ligand design is considered an interesting development in the field of AD therapeutics.^{4,25} Remarkably, while there are some precedents of chelators with additional $A\beta$ peptide intercalation ability and amyloid binding properties,^{20,26} the reverse strategy, i.e., the addition of chelating properties to compounds known to have strong affinity for amyloid fibrils, has attracted little attention.²⁰ However, this approach is substantiated by the use for decades of ThT and CR to stain amyloids such as $A\beta$ and by the accumulation of copper and zinc in cerebral amyloid deposits. It therefore has the potential to facilitate metal binding by improving targeting.

On the basis of the above premises, the development of metal-ion chelators with potential radiolabeling and antioxidant features from the traditional dye ThT is the main objective of this work. Integrating these properties without altering the main structural and aromatic features of ThT has led us to the molecular framework **M1** depicted in Figure 1. Compounds based on **M1** are unchanged as a result of the removal of the methyl group on the heterocyclic nitrogen of ThT. In accordance with the literature, this removal causes an increase in affinity for $A\beta$ fibrils as well as greater lipophilicity and therefore easier

crossing of the BBB.¹² In addition, it enables the nitrogen atom to act as an electron donor to metal ions. The second main difference between **M1** and ThT consists of the replacement of the dimethylaminophenyl moiety by a phenol or aniline ring, which has manifold consequences: the presence of the OH or NH_2 functional group at the position shown in Figure 1 makes **M1** suitable to act as a chelating ligand, provides it with potential antioxidant properties, and facilitates iodine substitution at the position para to the group, thus transforming **M1** into an iodine-labeled compound suitable for imaging.

The strategy we propose for the selection of compounds to be assayed as potential anti-AD agents makes use of several in silico tools. These allow the identification of commercial compounds that enclose the selected **M1** framework and fulfill

- (7) Chander, H.; Chauhan, A.; Chauhan, V. *J. Alzheimer's Dis.* **2007**, *12*, 261–269.
- (8) Krebs, M. R. H.; Bromley, E. H. C.; Donald, A. M. *J. Struct. Biol.* **2005**, *149*, 30–37.
- (9) Li, Q.; Min, J.; Ahn, Y.-H.; Namm, J.; Kim, E. M.; Lui, R.; Kim, H. Y.; Ji, Y.; Wu, H.; Winsniewski, T.; Chang, Y.-T. *ChemBioChem* **2007**, *8*, 1679–1687.
- (10) Maezawa, I.; Hong, H.-S.; Liu, R.; Wu, C.-Y.; Cheng, R. H.; Kung, M.-P.; Kung, H. F.; Lam, K. S.; Oddo, S.; LaFerla, F. M.; Jin, L.-W. *J. Neurochem.* **2008**, *104*, 457–468.
- (11) Partridge, W. M. *Drug Discovery Today* **2007**, *12*, 54–61.
- (12) Yona, R. L.; Mazères, S.; Faller, P.; Gras, E. *ChemMedChem* **2008**, *3*, 63–66.
- (13) Bush, A. I. *Neurobiol. Aging* **2002**, *23*, 1031–1038.
- (14) Bush, A. I. *Trends Neurosci.* **2003**, *26*, 207–214.
- (15) Bush, A. I.; Tanzi, R. E. *Proc. Natl. Acad. Sci. U.S.A.* **2002**, *99*, 7317–7319.
- (16) Cherny, R. A.; et al. *Neuron* **2001**, *30*, 665–676.
- (17) Crouch, P. J.; Barnham, K. J.; Bush, A. I.; White, A. R. *Drug News Perspect.* **2006**, *19*, 469–474.
- (18) Crouch, P. J.; White, A. R.; Bush, A. I. *FEBS Journal* **2007**, *274*, 3775–3783.
- (19) Cuajungco, M. P.; Frederickson, C. J.; Bush, A. I. *Subcell. Biochem.* **2005**, *38*, 235–254.
- (20) Dedeoglu, A.; Cormier, K.; Payton, S.; Tseitlin, K. A.; Kremsky, J. N.; Lai, L.; Li, X.; Moir, R. D.; Tanzi, R. E.; Bush, A. I.; Kowall, N. W.; Rogers, J. T.; Huang, X. *Exp. Gerontol.* **2004**, *39*, 1641–1649.
- (21) Huang, X.; Atwood, C. S.; Hartshorn, M. A.; Multhaup, G.; Goldstein, L. E.; Scarpa, R. C.; Cuajungco, M. P.; Gray, D. N.; Lim, J.; Moir, R. D.; Tanzi, R. E.; Bush, A. I. *Biochemistry* **1999**, *38*, 7609–7616.
- (22) Lee, J.-Y.; Friedman, J. E.; Angel, I.; Kozak, A.; Koh, J.-Y. *Neurobiol. Aging* **2004**, *25*, 1315–1321.
- (23) Bebbington, D.; Monck, N. J. T.; Gaur, S.; Palmer, A. M.; Benwell, K.; Harvey, V.; Malcolm, C. S.; Porter, R. H. P. *J. Med. Chem.* **2000**, *43*, 2779–2782.
- (24) Ji, H.-F.; Zhang, H.-Y. *Bioorg. Med. Chem. Lett.* **2005**, *15*, 21–24.
- (25) Schugar, H.; Green, D. E.; Bowen, M. L.; Scott, L. E.; Storr, T.; Bohmerle, K.; Thomas, F.; Allen, D. D.; Lockman, P. R.; Merkel, M.; Thompson, K. H.; Orvig, C. *Angew. Chem., Int. Ed.* **2007**, *46*, 1716–1718.
- (26) Cherny, R. A.; Barnham, K. J.; Lynch, T.; Volitakis, I.; Li, Q.-X.; McLean, C. A.; Multhaup, G.; Beyreuther, K.; Tanzi, R. E.; Masters, C. L.; Bush, A. I. *J. Struct. Biol.* **2000**, *130*, 209–216.

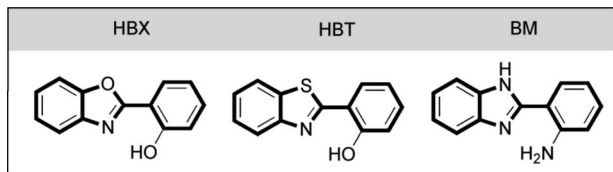


Figure 2. Selected commercial compounds.

the main biochemical requirements for Alzheimer's therapy at no time cost in experimental work. As a result of the virtual screening (VS) process described below, the three compounds 2-(2-hydroxyphenyl)benzoxazole (**HBX**), 2-(2-hydroxyphenyl)benzothiazole (**HBT**), and 2-(2-aminophenyl)-1*H*-benzimidazole (**BM**) (Figure 2) were selected for purchase. The syntheses of the corresponding iodinated derivatives and the determination of their abilities to coordinate Zn(II) and Cu(II) ions in the solid phase and in solution are reported in this work. These and subsequent biochemical assays, including their suitabilities for reducing the *in vitro* A β _{1–40} aggregation induced by Cu(II) and Zn(II) and their abilities to intercalate into synthetic human A β _{1–42} fibrils, show the potential of the new compounds for AD treatment.

Experimental Section

Materials. All of the solvents were reagent-grade and used without further purification unless otherwise specified. The commercial compounds **HBX**, **HBT**, **BM**, CQ, and ThT were purchased from Aldrich. Iodination reactions were carried out in the absence of light using MeOH and CH₂Cl₂ solvents freshly distilled over CaH₂. Milli-Q water was used to prepare all of the metal stock solutions. Absolute ethanol (HPLC–UV–IR quality) was obtained from Panreac. Sodium chloride, hydrochloric acid, and a standard solution of NaOH (0.5 M) were purchased from Sigma-Aldrich for the spectrophotometric titrations.

Instrumentation. ¹H and ¹³C NMR spectra of samples in CDCl₃ or CD₃OCD₃ solution at room temperature were recorded using a Bruker AC250 or AV-360 instrument. Electrospray ionization mass spectrometry (ESI-MS) was performed on a VG Quattro Micromass instrument using the following experimental conditions: 10 μ L of sample injected at 15 μ L min^{–1}; capillary counter electrode voltage, 4.5 kV; lens counter electrode voltage, 1.0 kV; cone potential, 55 V; source temperature, 90 °C; *m/z* range, 100–1600. The carrier was a 1:1 acetonitrile/water mixture or methanol containing 1–20% formic acid. Chemical ionization mass spectrometry (CI-MS) was performed on a ThermoFinnigan TRACE DSQ MS instrument using a direct-insertion probe. The samples were evaporated at 200 °C, and the ionization gas mixture was NH₃, the electron energy 70 eV, and the *m/z* range 100–900. Elemental analyses were performed on a Carlo-Erba CHNS EA-1108 analyzer. The EPR spectra were obtained using a Bruker ELEXYS E500 X-band spectrometer equipped with a variable-temperature unit, a field-frequency (F/F) lock accessory, and built-in NMR gaussmeter. A rectangular TE102 cavity was used for the measurements. Precautions to avoid undesirable spectral distortions and line broadenings, such as those arising from microwave power saturation and magnetic field over modulation, were also taken into account. To avoid dipolar line broadening from dissolved oxygen, the solutions were always carefully degassed with pure argon. The acidity and stability constants were spectrophotometrically determined in 50% EtOH/water solutions by means of an automatic titration system consisting of a Knick pH meter equipped with a Crison combined electrode. Electronic absorption spectra were recorded on a Hewlett-Packard 8452A diode array spectrophotometer over a 190–1100 nm range in a quartz flow cuvette with a path length of 10 mm. Titrations were carried out in a 50 mL double-walled vessel with continuous stirring, and a constant 0.10 M NaCl ionic strength was maintained

throughout each titration. The electrode was calibrated before each titration by titrating a known amount of aqueous HCl with NaOH using the same conditions under which the acidity and stability constants were measured. A Gran plot (measured mV vs calculated pH) gave a working slope and intercept for use in directly converting the measured potentiometric data into values of $-\log[H^+]$.²⁷ Microadditions of the carbonate-free 0.5 M NaOH stock solution were made using a Hamilton microburet controlled by an IBM-compatible PC by means of a locally written QBasic program. The temperature of the solution was kept constant at 37 \pm 0.2 °C by a Thermo Haake DC-10 circulator. The solution was continuously propelled by an Ismatec peristaltic pump at a flow rate of 2 mL min^{–1}. For the determination of the stability constants, the metal concentrations in the CuCl₂ and ZnCl₂ solutions were determined by titration with 0.10 M EDTA.²⁸

Database Selection, Substructure Searching, and Filtering Process. eMolecules (eMolecules, Inc.) is a free chemical structure search engine.²⁹ It contains about 8 million commercial compounds from more than 150 suppliers. The eMolecules Web site (<http://www.emolecules.com>) enables searching for a molecular structure by drawing it in the ChemWriter Java application.³⁰ The resulting molecules are depicted in a table with molecular properties and purchasing information. Filters 1–3 described below require the use of Instant JChem.³¹ The clogP value required for the calculation of log BB (filter 4) was determined using clogP version 4.0.³²

Iodination of HBX, HBT, and BM. All of the iodination reactions were carried out in the absence of light using freshly distilled solvents.

2-(Benzo[d]oxazol-2-yl)-4-iodophenol (HBXI). NaI (0.430 g, 2.86 mmol) was added to a solution of **HBX** (0.505 g, 2.39 mmol) in MeOH (15 mL). The reaction mixture was stirred at room temperature for \sim 5 min, after which a solution containing chloramine T (*N*-chloro-*p*-toluenesulfonamide, CAT) (1.30 g, 5.73 mmol) in the minimum volume of MeOH was added dropwise. The iodine color was lost after the last drop of oxidizing agent. Stirring was continued for \sim 2 h, after which the solvent was removed in vacuo. The residue was washed with abundant H₂O, and the resultant pale yellow solid was dissolved in the minimum amount of warm MeOH. Addition of diethyl ether then resulted in the appearance of a white solid. This suspension was kept at -4 °C for 12 h, yielding a white crystalline solid that was filtered off and dried under vacuum to afford the product **HBXI** (0.61 g, 76%). ¹H NMR (CHCl₃-*d*₁, 300 MHz): δ 11.5 (s, 1H), 8.33 (d, *J* = 1.8 Hz, 1H), 7.59–7.74 (m, 2H), 7.69 (dd, *J* = 8.7, 1.8 Hz, 1H), 7.35–7.40 (m, 2H), 6.92 (d, *J* = 8.7 Hz, 1H). ¹³C NMR (CHCl₃-*d*₁, 75.48 MHz): δ 80.5, 110.7, 112.8, 119.7, 125.2, 125.8, 135.3, 139.7, 141.9, 149.1, 158.3, 161.3. MS (+ESI-MS) *m/z* (relative intensity): 338.2 ([L + H]⁺, 100). Anal. Calcd (Found) for C₁₃H₈INO₂: C, 46.32 (46.20); H, 2.39 (2.29); N, 4.15 (4.03).

2-(Benzo[d]thiazol-2-yl)-4-iodophenol (HBTI). A mixture of NaI (0.390 g, 2.64 mmol), **HBT** (0.500 g, 2.19 mmol), and CAT (1.20 g, 5.27 mmol) was dissolved in 30 mL of MeOH and stirred at room temperature for 2 h. The solvent was then removed in vacuo and the solid obtained washed with 50 mL of water. The yellow solid obtained was recrystallized with 15 mL of CH₃CN, affording **HBTI** as a yellow pale solid (0.47 g, 61%). ¹H NMR (CHCl₃-*d*₁, 300 MHz): δ 12.2 (s, 1H), 7.99 (d, *J* = 1.9 Hz, 1H), 7.95–7.99 (m, 2H), 7.65 (dd, *J* = 8.6, 1.9 Hz, 1H), 7.44–7.56 (m, 2H), 6.88

(27) Gran, G. *Analyst* **1952**, 77, 661–671.

(28) *A Text-Book of Quantitative Inorganic Analysis*; Vogel, A. I., Ed.; Longmans Green & Co.: London, 1961.

(29) eMolecules, Inc. eMolecules Web site. <http://www.emolecules.com> (accessed Dec 29, 2008).

(30) Metamolecular, LLC. ChemWriter Web page. <http://metamolecular.com/chemwriter/> (accessed Dec 29, 2008).

(31) *Instant JChem*, version 2.2.1; ChemAxon Kft.: Budapest, 2008; <http://www.chemaxon.com> (accessed Dec 29, 2008).

(32) *ClogP*, version 4.0 for Windows; BioByte Corporation: Claremont, CA, 1999; <http://www.biobyte.com/bb/prod/clogp40.html> (accessed Dec 29, 2008).

(d, $J = 8.6$ Hz, 1H). ^{13}C NMR (CHCl_3 - d_1 , 75.48 MHz): δ 80.2, 120.1, 121.5, 122.2, 122.3, 125.8, 126.2, 126.8, 132.4, 136.3, 140.9, 156.6, 167.5. MS (+ESI-MS) m/z (relative intensity): 354.2 ($[\text{L} + \text{H}]^+$, 100). Anal. Calcd (Found) for $\text{C}_{13}\text{H}_8\text{INO}$: C, 44.21 (44.17); H, 2.28 (2.10); N, 3.97 (3.80); S, 9.08 (8.89).

2-(1H-Benzo[d]imidazol-2-yl)-4-iodoaniline (BMI). **BM** (0.492 g, 2.34 mmol) was dissolved in anhydrous CH_2Cl_2 (30 mL). A solution of bis(pyridine)iodonium(I) tetrafluoroborate ($[\text{Py}_2]\text{BF}_4$) (1.04 g, 2.81 mmol) in CH_2Cl_2 was added dropwise, whereupon the solution turned pink. The resultant mixture was stirred at room temperature for 2 h, and the resultant pale-white solid formed was collected by filtration and washed with 5% aqueous sodium thiosulfate (10 mL) and water (25 mL). The solid obtained was recrystallized with 20 mL of CH_3OH , affording **BMI** as a white solid (0.49 g, 62%). ^1H NMR (CH_3COCH_3 - d_6 , 300 MHz): δ 8.33 (d, $J = 2.0$ Hz, 1H), 7.75–7.66 (m, 2H), 7.66 (s, 1H), 7.57 (s, 1H), 7.53 (dd, $J = 2.0$, 8.5 Hz, 1H), 7.27–7.19 (m, 2H), 6.74 (d, $J = 8.5$ Hz, 1H), 6.50 (s, 1H). ^{13}C NMR (CH_3COCH_3 - d_6 , 75.48 MHz): δ 79.8, 98.0, 113.1, 116.1, 118.5, 120.8, 123.6, 123.9, 134.1, 141.0, 143.9, 145.1, 147.1. MS (+ESI-MS) m/z (relative intensity): 336.2 ($[\text{L} + \text{H}]^+$, 100). Anal. Calcd (Found) for $\text{C}_{13}\text{H}_{10}\text{IN}_3$: C, 46.59 (46.58); H, 3.01 (2.96); N, 12.54 (12.37).

General Procedure for the Synthesis of ML_2 [$\text{M} = \text{Cu(II)}$, **Zn(II); $\text{L} = \text{BXXI}$, **BTI**].** A solution containing 2 equiv of the protonated ligand HL ($\text{HL} = \text{HBXXI}$, **HBTI**) in the minimum volume of MeOH was added to a solution of MCl_2 [$\text{M} = \text{Cu(II)}$, **Zn(II)**] in MeOH (2–5 mL). The reaction mixture was stirred at room temperature for ~ 10 min, after which a few drops of Et_3N were added. The resultant mixture was stirred for ~ 1 h, and the solid obtained was isolated and purified according to the procedure described below for each compound under the corresponding heading.

[Cu(BXI) $_2$]. $\text{CuCl}_2 \cdot 6\text{H}_2\text{O}$ (0.025 g, 0.15 mmol) in MeOH (5 mL) and **HBXI** (0.10 g, 0.29 mmol) in MeOH (25 mL) were used as described above. The resultant dark solution was left to stand at -30°C for ~ 12 h. The dark-brown solid formed was collected by filtration, washed with MeOH, and dried in vacuo, yielding **[Cu(BXI) $_2$]** (0.089 g, 81%). MS (–CI-MS): m/z 735.1 [M^-]. Anal. Calcd (Found) for $\text{C}_{26}\text{H}_{14}\text{CuI}_2\text{N}_2\text{O}_4$: C, 42.44 (42.07); H, 1.92 (1.83); N, 3.81 (3.63).

[Zn(BXI) $_2$]. ZnCl_2 (0.019 g, 0.14 mmol) in MeOH (5 mL) and **HBXI** (0.094 mg, 0.28 mmol) in MeOH (25 mL) were used as described above. The resultant yellow precipitate was collected by filtration, washed with MeOH, and dried in vacuo to afford **[Zn(BXI) $_2$]** as a pale-yellow powder (0.093 g, 90%). MS(–CI-MS): m/z 735.7 [M^-]. Anal. Calcd (Found) for $\text{C}_{26}\text{H}_{14}\text{ZnI}_2\text{N}_2\text{O}_4$: C, 42.34 (42.21); H, 1.91 (1.82); N, 3.80 (3.65).

[Cu(BTI) $_2$]. $\text{CuCl}_2 \cdot 6\text{H}_2\text{O}$ (0.036 g, 0.21 mmol) in MeOH (5 mL) and **HBTI** (0.15 g, 0.42 mmol) in MeOH (25 mL) were used as described above. A dark solution and dark-brown solid formed upon mixing, and the reaction mixture was left to stand at -30°C for ~ 12 h. The precipitate was collected by filtration, washed with MeOH, and dried in vacuo, yielding **[Cu(BTI) $_2$]** as a dark-brown powder (0.121 g, 75%). MS (–CI-MS): m/z 766.7 [M^-]. Anal. Calcd (Found) for $\text{C}_{26}\text{H}_{14}\text{CuI}_2\text{N}_2\text{O}_2\text{S}_2$: C, 40.67 (40.39); H, 1.84 (1.76); N, 3.65 (3.52); S, 8.35 (8.10).

[Zn(BTI) $_2$]. ZnCl_2 (0.029 g, 0.21 mmol) in MeOH (5 mL) and **HBTI** (0.15 g, 0.42 mmol) in MeOH (25 mL) were used as described above. The resultant yellow precipitate was collected by filtration, successively washed with MeOH and Et_2O , and dried in vacuo to afford **[Zn(BTI) $_2$]** as a pale yellow powder (0.14 g, 87%). Negative CI-MS: m/z 767.9 [M^-]. Anal. Calcd (found) for $\text{C}_{26}\text{H}_{14}\text{ZnI}_2\text{N}_2\text{O}_2\text{S}_2$: C, 40.57 (40.41); H, 1.83 (1.79); N, 3.64 (3.52); S, 8.50 (8.35).

General Procedure for the Synthesis of $[\text{M}(\text{BMI})_2]\text{Cl}_2$ [$\text{M} = \text{Cu(II)}$, **Zn(II)].** A solution containing 2 equiv of the ligand **BMI** in the minimum volume of CH_3CN was added to a solution of MCl_2 [$\text{M} = \text{Cu(II)}$, **Zn(II)**] in CH_3CN (2–5 mL). The reaction mixture

was stirred at room temperature for 2 h, and the resultant suspension was treated as indicated below.

[Cu(BMI) $_2$] Cl_2 . $\text{CuCl}_2 \cdot 6\text{H}_2\text{O}$ (0.038 g, 0.22 mmol) in CH_3CN (5 mL) and **BMI** (0.15 g, 0.45 mmol) in CH_3CN (25 mL) were used as described above. The resultant dark-green suspension was left to stand at -30°C for ~ 1 h. The precipitate was collected by filtration, washed with CH_3CN , and dried in vacuo, yielding **[Cu(BMI) $_2$] Cl_2** as a dark-green powder (0.141 g, 80%). MS (+ESI-MS) m/z (relative intensity): 733.3 ($[\text{M} - 2\text{Cl}]^+$, 100). Anal. Calcd (Found) for $\text{C}_{26}\text{H}_{20}\text{CuI}_2\text{N}_6\text{Cl}_2$: C, 38.80 (38.75); H, 2.51 (2.42); N, 11.44 (11.21).

[Zn(BMI) $_2$] Cl_2 . ZnCl_2 (0.030 g, 0.22 mmol) in CH_3CN (5 mL) and **BMI** (0.15 g, 0.45 mmol) in CH_3CN (25 mL) were used as described above. The resultant yellowish suspension was kept at -30°C for 1 h. The precipitate was collected by filtration, washed with warm CH_3CN , and dried in vacuo to afford **[Zn(BMI) $_2$] Cl_2** as a pale-white powder (0.164 g, 92%). MS (+ESI-MS) m/z (relative intensity): 734.4 ($[\text{M} - 2\text{Cl}]^+$, 100). Anal. Calcd (Found) for $\text{C}_{26}\text{H}_{20}\text{ZnI}_2\text{N}_6\text{Cl}_2$: C, 38.72 (38.40); H, 2.50 (2.48); N, 10.42 (10.11).

X-ray Crystallography. Crystals of **HBXI** and **HBTI** were grown from concentrated methanol/acetone solutions of the respective compounds, whereas crystals of **BMI** were obtained via slow evaporation of a concentrated acetone solution. The crystals were mounted on glass fibers, and measurements were made on a Bruker SMART-APEX CCD area-detector diffractometer at room temperature with graphite-monochromatized Mo K α radiation. Lorentz polarization and absorption corrections were applied using Bruker SAINT³³ and SADABS³⁴ software. Structures were solved by direct methods and refined by full-matrix least-squares on F^2 for all unique measured data using SHELXTL.³⁵ Non-hydrogen atoms were refined anisotropically. Hydrogen atoms bonded to carbon were included with riding-model constraints and isotropic displacement parameters equal to 1.2 times the U_{eq} values of the corresponding carbon atoms. Hydrogen atoms bonded to heteroatoms were localized in a Fourier map and refined with constraints (**HBXI** and **HBTI**) or restraints (**BMI**) and isotropic displacement parameters equal to 1.5 times the U_{eq} values of the corresponding heteroatoms. Relevant crystal data, data collection, and refinement parameters are summarized in Table S1 and the CIF files in the Supporting Information.

DFT Calculations. Full geometry optimizations and harmonic frequency calculations were performed using density functional theory (DFT) with the nonlocal hybrid B3LYP^{36,37} functional, a robust and well-tested functional that has been successfully used for a great variety of systems, including open-shell Cu(II) complexes with saturated coordination environments and similar spin density distributions. All of the calculations were carried out using the following basis sets: For Cu and Zn, we used Wachter's primitive set (14s9p5d),³⁸ supplemented with one s, two p, and one d diffuse function³⁹ and one f polarization function, the final basis set being (15s11p6d1f)/[10s7p4d1f]. The standard 6-31++G(d,p) basis set was used for C, N, O, and H. The photophysical properties of the selected ligands were studied using the time-dependent DFT (TDDFT) formalism.^{40,41} First singlet excited state (S_1) energies were obtained with TDDFT at the geometries of the first electronic

(33) SAINT, version 6.22; Bruker AXS Inc.: Madison, WI, 2001.

(34) Sheldrick, G. M. SADABS, version 2.03; University of Göttingen: Göttingen, Germany, 2002.

(35) Sheldrick, G. M. SHELXTL, version 6.10; Bruker AXS Inc.: Madison, WI, 2000.

(36) Becke, A. D. *J. Chem. Phys.* **1993**, *98*, 5648–5652.

(37) Lee, C.; Yang, W.; Parr, R. G. *Phys. Rev. B* **1988**, *37*, 785–789.

(38) Wachters, A. J. H. *J. Chem. Phys.* **1970**, *52*, 1033–1036.

(39) Hay, P. J. *J. Chem. Phys.* **1977**, *66*, 4377–4384.

(40) Stratmann, R. E.; Scuseria, G. E.; Frisch, M. J. *J. Chem. Phys.* **1998**, *109*, 8218–8224.

(41) Bauernschmitt, R.; Haeser, M.; Treutler, O.; Ahlrichs, R. *Chem. Phys. Lett.* **1997**, *264*, 573–578.

triplet states. Previous studies⁴² have shown that UB3LYP geometries of the lowest triplet states arising from the same HOMO → LUMO excitation energy as S_1 provide $S_0 \rightarrow S_1$ excitation energies that are very similar to those obtained from the more computationally demanding singlet TDDFT reoptimizations. All of the calculations were performed using the Gaussian 03 set of programs.⁴³

UV–Vis Determination of Acidity and Stability Constants.

Since the compounds **HBXI**, **HBTI**, and **BMI** are slightly soluble in water, ethanolic 1 mM stock solutions were prepared. In each titration, the solvent composition in the vessel was 50% (v/v) ethanol/water. For each compound, the acidity constant was determined by titrating a 0.024 mM solution of the compound with microadditions of 0.5 M NaOH standard solution, recording the UV–vis spectrum at each titration point. At least 30 spectra were taken in the pH range 2–11. The data were analyzed by importing both the absorbance and pH values into the pHab2000 computer program,⁴⁴ which calculates acidity constants by means of a linear least-squares curve-fitting analysis. For the sake of comparison, acidity constants for clioquinol (0.12 mM), denoted as HCQ throughout the solution equilibria studies, were also determined using the same methodology. The stability constants for the Cu(II) and Zn(II) complexes with **BXI**, **BTI**, and **BMI** were also determined by UV–vis pH titrations under the same conditions as outlined above. The ligand-to-metal molar ratios used in the experiments were 1:1 and 2:1 for each ligand with $M = \text{Cu(II)}$ or Zn(II) . For each titration, at least 30 spectra were recorded in the pH range 2–12. As with the pK_a values, the stability constants were calculated with the pHab2000 computer program. Speciation diagrams for the free ligands and the corresponding complexes [$M = \text{Cu(II)}$ or Zn(II) ; $L = \text{HBXI}$, **HBTI**, **BMI** and HCQ] were calculated using the program HySS2006.⁴⁵

A β Turbidity Measurements. Turbidity assays were performed following a previously described procedure⁴ with some variations. Briefly, synthetic A β_{1-40} amyloid peptide (Biopeptide Co., Inc.), was prepared in distilled, deionized water at $\sim 200 \mu\text{M}$. To obtain monomeric peptide as the starting material, the solution was sonicated three times and then filtered through a $0.2 \mu\text{m}$ syringe filter (Millipore) to eliminate any remaining aggregate. An extinction coefficient of $1450 \text{ cm}^{-1} \text{ M}^{-1}$ at 276 nm was used to measure the concentration of monomeric A β_{1-40} . Two 4-(2-hydroxyethyl)-1-piperazineethanesulphonic acid (HEPES) buffer solutions (20 μM) containing 150 μM NaCl were prepared with distilled, deionized water at pH values of 6.6 and 7.4. These solutions were treated overnight with 5% (w/v) Chelex and filtered through $0.22 \mu\text{m}$ acetate filters (Millipore). Stock solutions of Cu(II) and Zn(II) were prepared from standards to final concentrations of 200 μM using the buffers at pH 6.6 and 7.4, respectively. Solutions of the different compounds tested [**HBXI**, **HBTI**, **BMI**, EDTA, CQ, Pittsburgh compound B (PIB), and ThT] were prepared in ethanol to final concentrations of 200 μM . The assay was performed by adding the A β_{1-40} peptide (25 μM) into a solution containing 25% ethanol and either ligand (50 μM), metal ion (25 μM), or both. Assays with no metal added were carried out at pH 6.6. The solutions were incubated overnight at 37 °C with constant agitation to accelerate peptide aggregation. The 405 nm absorbance of the evenly suspended aggregates was measured in a Cary-100 Varian spectrophotometer. Each sample was measured four times and shaken between each measurement. Each spectrophotometric value was corrected for the blank containing HEPES buffer and the respective ligand, metal, or ligand–metal mixture.

CD Measurements. Samples were prepared as described in A β Turbidity Measurements. Circular dichroism (CD) measurements

were performed with a Jasco 715 UV–vis spectropolarimeter equipped with a Peltier temperature control system using a 1 mm path length silica quartz cuvette (Hellma). Agitated and evenly suspended samples were measured at 25 °C within the wavelength range 200–250 nm with a 1 nm step resolution and an integration time of 2 s. All of the spectra are shown as an average of five baseline-corrected scans from which the buffer-plus-metal spectra were subtracted.

Amyloid Fibril Formation. Lyophilized synthetic human A β_{1-42} amyloid and a 20-residue synthetic fragment ranging from Q10 to S29 of islet amyloid polypeptide (IAPP), obtained from Biopeptide Co. and EZBiolab, Inc., respectively, were used as amyloid-forming protein models. The peptides were dissolved in hexafluoro-2-propanol (HFIP) to a final concentration of 2%, and aliquots of this solution in the appropriate volumes were used in the subsequent assays. After evaporation of the HFIP, the dried peptides were stored at $-80 \text{ }^\circ\text{C}$. In order to generate A β_{1-42} or IAPP_{10–20} fibrils, the peptides were redissolved in DMSO and aggregation initiated by adding phosphate buffered saline (PBS, pH 7.4) or 10 mM sodium acetate (pH 5.5), respectively, to reach final concentrations of 2.5% DMSO and 100 μM peptide. The solutions were incubated for 24 h at room temperature to allow for the formation of mature amyloid fibrils. The presence of fibrils was tested by transmission electron microscopy (data not shown).

Fluorescence Microscopy Binding Assays. Mature fibrils in 2.5% DMSO and either PBS or 10 mM acetate were incubated with a 1 mg/mL ligand solution dissolved in ethanol at a final ratio of 4:1 (v/v) for 10 min at room temperature. The fibrils were cleaned twice with doubly distilled water and then suspended again in water before their analysis under UV light. Positive binding controls were incubated under the same conditions with ThT (1 mg/mL in PBS or 10 mM sodium acetate), with ethanol added to reach a final concentration of 20% (v/v) ethanol/water. In negative binding controls, a 1 mg/mL solution of bovine serum albumin (BSA) replaced the fibril solution. Images were obtained with an excitation filter ranging from 515 to 566 nm and an emission filter that collects light with a wavelength longer than 580 nm, using a Leica DMBR microscope under a $100\times$ or $40\times$ lens and 2.53 s exposure.

Fluorescence Measurements. All of the measurements were recorded in a fluorescence spectrophotometer (Varian, Cary Eclipse) at 293 K and 2.5 nm \times 5 nm excitation and emission slit widths. Mature fibrils prepared as mentioned above were diluted $10\times$ in 10 mM sodium acetate solution (pH 5.5) containing the ligand at 0.1 mg/mL. Fluorescence data were collected after 5 min to ensure that thermal equilibrium had been achieved. Positive binding controls were performed with ThT in 10 mM sodium acetate (pH 5.5) at a final concentration of 20 μM .

Results and Discussion

Selection of Commercial Compounds Enclosing the Molecular Framework M1 by Virtual Screening Methods. VS methods are widely used in drug discovery processes in order to reduce costs and time.^{46–49} In this study, the application of these methods involved two main steps: (1) searching through the selected commercial database for structures that enclose **M1** and (2) filtering the resultant list of molecules so the selected commercial compounds fulfill the most common druglike properties and have lipophilicities adequate for crossing the BBB. As a result, three compounds (**HBX**, **HBT**, and **BM**) were finally selected as potential candidates. The software used is

(42) Casadesus, R.; Vendrell, O.; Moreno, M.; Lluch, J. M.; Morokuma, K. *Chem. Phys.* **2006**, *325*, 243–250.

(43) Frisch, M. J.; et al. Gaussian, Inc.: Wallingford, CT, 2004.

(44) Gans, P.; Sabatini, A.; Vacca, A. *Ann. Chim.* **1999**, *89*, 45–49.

(45) Alderighi, L.; Gans, P.; Ienco, A.; Peters, D.; Sabatini, A.; Vacca, A. *Coord. Chem. Rev.* **1999**, *184*, 311–318.

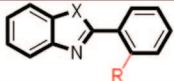
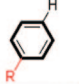
(46) Walters, W. P.; Stahl, M. T.; Murcko, M. A. *Drug Discovery Today* **1998**, *3*, 160–178.

(47) Waszkowycz, B. *Drug Discovery Today* **2008**, *13*, 219–226.

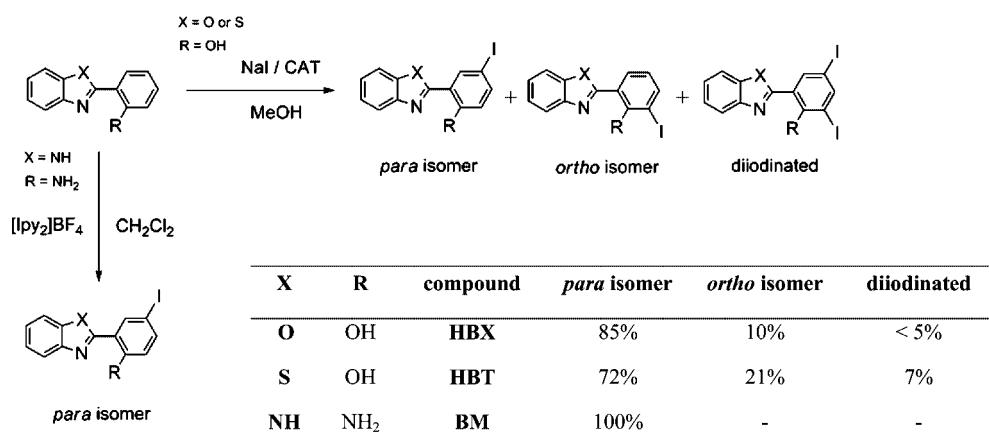
(48) Lengauer, T.; Lemmen, C.; Rarey, M.; Zimmermann, M. *Drug Discovery Today* **2004**, *9*, 27–34.

(49) Merlot, C.; Domine, D.; Cleve, C.; Church, D. J. *Drug Discovery Today* **2003**, *8*, 594–602.

Table 1. Numbers of Commercial Compounds that Enclose **M1** and Fulfill the Subsequent Constraints Imposed

M1							
X		O		S		N	
R		OH	NH ₂	OH	NH ₂	OH	NH ₂
number of commercial cpds ^[a]		1986	9	804	11	61	10
Filter 1		676	6	247	4	16	5
Filter 2	MW ≤ 450	398	6	173	2	15	5
Filter 3	Lipinski's rules ^[b]	300	6	81	2	15	5
Filter 4	Log BB ^[c]	19	5	5	0	5	2

^a From the eMolecules commercial database. ^b Lipinski's rules: clogP ≤ 5; HBD ≤ 5; HBA ≤ 10 (HBD and HBA are defined in the text). ^c Log BB = −0.0148 TPSA + 0.139 clogP + 0.152, where the TPSA and clogP parameters are defined in the text.

Scheme 1. Iodination of **HBX**, **HBT**, and **BM** and Yields Estimated from NMR Data

described in the Experimental Section, and the results obtained are given in Table 1.

Of the various alternatives assayed, the eMolecules database was considered the most appropriate choice. The filters shown in Table 1 were subsequently applied to the commercial compounds enclosing **M1** (Figure 1). Filter 1 establishes that no functional group can be placed para to R, in order to allow iodination of the aromatic ring. Filters 2, 3, and 4 ensure that the resultant molecules fulfill druglike criteria. These are most commonly defined using Lipinski's rules: molecular weight (MW) less than 500, the calculated logarithm of the octanol–water partition coefficient (clogP) less than 5, the number of hydrogen-bond donor atoms (HBD) less than 5, and the number of hydrogen-bond acceptor atoms (HBA) less than 10.⁵⁰ As more restrictive terms have been established for the MW in order to ensure brain permeation,^{51,52} filter 3 retains compounds that satisfy the set of values: MW ≤ 450, clogP ≤ 5, HBD ≤ 5, and HBA ≤ 10. Filter 4 involves calculation of log BB, a common measure of the degree of BBB penetration, by means of the equation shown in footnote ^c of Table 1. This equation has shown good predictive ability and comprises two simple variables that can be rapidly computed for any structure: clogP

and the topological polar surface area (TPSA).^{53,54} The numbers of various types of commercial compounds that satisfied all of the constraints are indicated in Table 1. The structures and log BB values of the final 36 candidates are shown in Figure S1 in the Supporting Information. The main criteria for selecting the molecules to be purchased were molecular simplicity and a log BB value greater than −0.3.⁵⁵ As a result, **HBX**, **HBT**, and **BM** (Figure 2) were selected as the initial compounds. The results obtained with these molecules should influence possible improvements and thus their replacement by other family members with finely tuned physicochemical and/or pharmacokinetic properties.

Chelating Properties of Compounds HBXI, HBTI, and BMI toward Cu(II) and Zn(II). Iodination of **HBX**, **HBT**, and **BM**. The iodination of aromatic compounds is a subject of continuing interest because of the extensive use of iodinated derivatives as imaging agents in noninvasive medical diagnostic techniques.^{56,57} The methodologies currently available for the preparation of iodophenols and iodinated aromatic amines are

(50) Lipinski, C. A.; Lombardo, F.; Dominy, B. W.; Feeney, P. J. *Adv. Drug Delivery Rev.* **1997**, *23*, 3–25.

(51) Clark, D. E.; Pickett, S. D. *Drug Discovery Today* **2000**, *5*, 49–58.

(52) van de Waterbeemd, H.; Camenisch, G.; Folkers, G.; Chretien, J. R.; Raevsky, O. A. *J. Drug Targeting* **1998**, *6*, 151–165.

(53) Clark, D. E. *J. Pharm. Sci.* **1999**, *88*, 815–821.

(54) Goodwin, J. T.; Clark, D. E. *J. Pharmacol. Exp. Ther.* **2005**, *315*, 477–483.

(55) Mestres, J., personal communication.

(56) Kung, H. F.; Newman, S.; Choi, S. R.; Oya, S.; Hou, C.; Zhuang, Z. P.; Acton, P. D.; Plossl, K.; Winkler, J.; Kung, M. P. *J. Med. Chem.* **2004**, *47*, 5258–5264.

(57) Bennacef, I.; Tymciu, S.; Dhilly, M.; Lasne, M.-C.; Debruyne, D.; Perrio, C.; Barré, L. *Bioorg. Med. Chem.* **2004**, *12*, 4533–4541.

based on reactions with a broad range of iodinating agents, among which the oxidation reaction with CAT is a very common method for ^{123}I labeling.^{58–60} Notwithstanding this, the reaction of CAT with the three selected molecules **HBX**, **HBT**, and **BM**, as shown in Scheme 1, gave satisfactory results only for the first two compounds. For the third one, **BM**, a different approach involving direct iodination with $[\text{Ipy}_2]\text{BF}_4$ led to the corresponding iodinated compound.^{61,62} In each of these procedures, the reaction proceeds at room temperature with a short reaction time and good yield. However, the reaction products obtained were different, as shown in Scheme 1. In the reaction of CAT with **HBX** and **HBT**, the iodination occurred at the positions ortho and para to the OH group, with a clear predominance of the latter isomer. In both cases, small amounts of diiodinated derivatives in the crude product of the reaction were also detected by NMR analysis. However, the synthetic procedure for **HBXI** and **HBTI** described in the Experimental Section allowed the isolation of the corresponding pure para isomer. Remarkably, the iodination reaction of **BM** with $[\text{Ipy}_2]\text{BF}_4$ afforded the *para*-iodo derivative as the single reaction product.

Structural Properties of HBXI, HBTI, and BMI from X-ray Data and DFT Calculations. Before the chelating and intercalation properties of the chosen ligands were evaluated, it was important to analyze their structural properties. For this purpose, the crystal structures of the three selected ligands (**HBXI**, **HBTI**, and **BMI**) were established by X-ray diffraction (Table S1 in the Supporting Information). The main features of the molecular structures, which are shown in Figure 3, are very similar to those of the parent noniodinated compounds.^{63–65} For this reason, only the distances and angle related to the intramolecular hydrogen bond between the two moieties linked by a single C–C bond are given for each compound in Table 2. As discussed below, these parameters are relevant for the fluorescence properties of these compounds. **HBXI** and **HBTI** molecules are roughly planar, with dihedral angles between the benzoxazole/benzothiazole and the phenol moiety of 4.6(2) and 5.1(1)°, respectively. In the case of compound **BMI**, however, the benzimidazole and aniline moieties are not coplanar, and the dihedral angle between them is 24.4(2)°. The difference in the dihedral angle is less pronounced when the values for the parent noniodinated compounds are compared: 3.1, 2.3, and 7.2° for **HBX**, **HBT**, and **BM**, respectively, as reported in previous studies.^{63–65} The intramolecular hydrogen bonds in the **HBXI**, **HBTI**, and **BMI** molecules involve the N(sp²) of the heterocyclic five-membered ring and the O–H (**HBXI** and **HBTI**) or N–H (**BMI**) group. Similar intramolecular hydrogen bonds are present in the parent compounds, even though in the case of **HBX**, the unit cell includes a second planar conformer with an intramolecular O–H...O hydrogen bond. Unlike **HBXI** and **HBTI**, the **BMI** crystal structure shows additional intermolecular N–H...N interactions involving the NH₂ and NH groups. Interestingly, in this latter compound, the NH₂ group shows a pyramidal disposition.

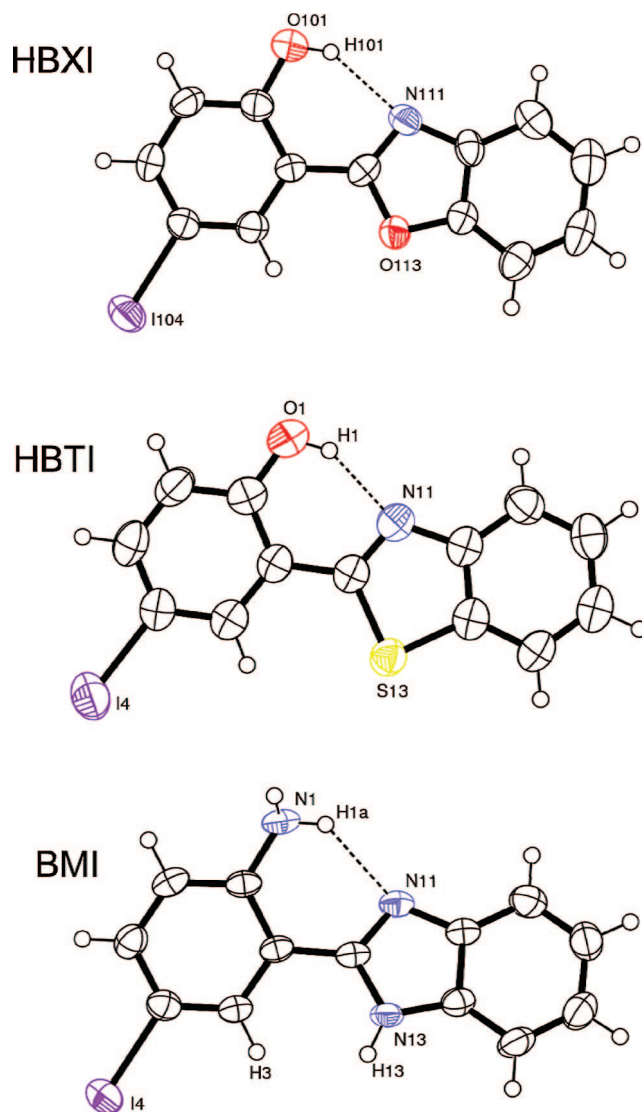


Figure 3. Ellipsoid plots (50% probability) for **HBXI**, **HBTI**, and **BMI**.

Table 2. Geometries (Distances in Å, Angle in deg) of the Intramolecular Hydrogen Bonds in **HBXI**, **HBTI**, and **BMI** according to X-ray Data and DFT Calculations

	HBXI			
	O101–H101	O101...N111	H101...N111	O101–H101...N111
X-ray	0.94 ^a	2.718(7)	1.90 ^a	145 ^a
DFT	0.99	2.670	1.80	145

	HBTI			
	O1–H1	O1...N11	H1...N11	O1–H1...N11
X-ray	0.94 ^a	2.606(5)	1.77 ^a	146 ^a
DFT	0.99	2.625	1.74	146

	BMI			
	N1–H1a	N1...N11	H1a...N11	N1–H1a...N11
X-ray	1.03 ^a	2.799(4)	2.10 ^a	123 ^a
DFT	1.01	2.730	1.94	132

^a Values normalized in accordance with ref 96.

In order to determine whether or not the conformation obtained by X-ray diffraction arises from packing effects or

(58) Hunter, W. M.; Greenwood, F. C. *Nature* **1962**, *194*, 495–496.

(59) Bolton, A. E.; Hunter, W. M. *Biochem. J.* **1973**, *133*, 529–539.

(60) Greenwood, F. C.; Hunter, W. M.; Glover, J. S. *Biochem. J.* **1963**, *89*, 114–123.

(61) Barluenga, J.; González, J. M.; García-Martín, M. A.; Campos, P. J.; Asensio, G. *J. Org. Chem.* **1993**, *58*, 2058–2060.

(62) Ezquerro, J.; Pedregal, C.; Lamas, C.; Barluenga, J.; Pérez, M.; García-Martín, M. A.; González, J. M. *J. Org. Chem.* **1996**, *61*, 5804–5812.

(63) Das, T. M.; Rao, C. P.; Kalle, N.; Rissanen, K. *Indian J. Chem.* **2003**, *42B*, 661–665.

(64) Stenson, P. *Acta Chem. Scand.* **1970**, *24*, 3729–3738.

(65) Tong, Y. P. *Acta Crystallogr.* **2005**, *E61*, o3076–o3078.

Table 3. Acidity Constants of the **HBXI**, **HBTI**, **BMI**, and **HCQ** Ligands and Stability Constants of their **Cu(II)** and **Zn(II)** Complexes, as Determined by Spectrophotometric Measurements in 0.10 M NaCl at 310 K (Errors Are for the Last Digit), and Calculated Values of pM $\{-\log[M]_{\text{free}}, \text{ where } M = \text{Cu(II)} (\text{pH} = 6.6) \text{ or } \text{Zn(II)} (\text{pH} = 7.4)\}$ for Solutions with $[M]_{\text{tot}} = 25 \mu\text{M}$ and $[\text{Ligand}]_{\text{tot}} = 50 \mu\text{M}$

ligand	ligand data ^a		Cu(II) data ^b			Zn(II) data ^b		
	pK_{a1}	pK_{a2}	$\log \beta_1$	$\log \beta_2$	$p\text{Cu}$	$\log \beta_1$	$\log \beta_2$	$p\text{Zn}$
HBXI	— ^c	9.978(9)	14.444(9)	23.06(7)	11.06	13.55(8)	22.25(9)	10.98
HBTI	— ^c	8.11(1)	12.049(9)	20.29(2)	10.52	11.68(1)	19.68(4)	10.91
BMI	3.650(2)	7.440(8)	10.347(9)	19.19(2)	9.46	10.87(7)	18.53(7)	10.55
HCQ	1.94(5)	8.300(2)	12.48(4)	21.91(3)	10.77	12.141(8)	20.23(1)	11.22

^a The acidity constants correspond to the following reactions (charges are omitted for the sake of clarity): $\text{H}_2\text{L} \rightleftharpoons \text{HL} + \text{H}$ (pK_{a1}); $\text{HL} \rightleftharpoons \text{L} + \text{H}$ (pK_{a2}). ^b The stability constants correspond to the following reactions (charges are omitted for the sake of clarity): $\text{M(II)} + \text{L} \rightleftharpoons \text{ML}$ ($\log \beta_1$); $\text{M(II)} + 2\text{L} \rightleftharpoons \text{ML}_2$ ($\log \beta_2$). ^c The pK_{a1} value is too low to be determined within the pH range studied.

reflects the intrinsic chemical properties of the molecule, we performed gas-phase calculations for the three ligands at the B3LYP/6-31++G(d,p) level of theory. As shown in Table 2, the **HBXI**, **HBTI**, and **BMI** molecules all present an intramolecular hydrogen bond between the two moieties that is consistent with the X-ray data. As a consequence of this interaction, both **HBXI** and **HBTI** have C_s symmetry in the gas phase, with the two rings therefore lying in the same plane. However, calculations for **BMI** indicate that the molecule slightly deviates from C_s symmetry, probably due to the steric repulsion between the two closest H atoms, H3 and H13, of the two moieties (Figure 3). This leads to a torsional angle of 5° around the single C—C bond. This result is in contrast to that found in the X-ray crystal structure, which indicates that this angle is 24° (see above). Since the X-ray data and DFT calculations for the parent compound **BM** afford a much smaller torsional angle (7° and 5° , respectively), it appears that packing effects in the crystal structure of **BMI** due to the iodine atom are responsible for this significant deviation from planarity (24°). Except for this difference, the molecular structures provided by X-ray diffraction and DFT calculations are in good agreement, and the trends in the hydrogen-bond distances are the same. That is, both DFT and X-ray diffraction determine that the ligand with the shortest intramolecular H-bond distance is **HBTI** whereas the one with the longest H-bond distance is **BMI**. This finding is consistent with the fact that NH_2 is a poorer H-bond donor than OH. The difference in the O—H \cdots N distances observed in **HBTI** and **HBXI** could be due either to the influence of sulfur or oxygen on the basicity of the N(sp^2) atom of the benzothiazole or benzoxazole moiety, respectively, or to geometric factors imposed by the different sizes of the heteroatoms O and S. Finally, it is also worth noting that as in the crystal structure, the exocyclic N in **BMI** is somewhat pyramidalized.

Acidity Constants of Compounds **HBXI**, **HBTI**, and **BMI**.

All of the iodinated ligands **HBXI**, **HBTI**, and **BMI** were investigated by UV–vis spectrophotometry to determine their ability to act as **Cu(II)** and **Zn(II)** chelators. To that end, spectrophotometric titrations to find the corresponding acidity constants (K_a) within the pH range 2–11 (Table 3) were first completed, and the results were used for the **Cu(II)** and **Zn(II)** metal binding studies. As an example, the set of variable-pH UV–vis experiments for **HBTI** is shown in Figure 4, while those for **HBXI** and **BMI** are given in Figures S2 and S3, respectively, in the Supporting Information. From these data, only one pK_a value was observed for **HBXI** and **HBTI**, which should be assigned to the deprotonation of the phenol moiety, consistent with the bathochromic shift of the absorption band corresponding to the aromatic $\pi \rightarrow \pi^*$ transition. In the same pH range, two pK_a values were observed for the **BMI** ligand, thus indicating formation of the diprotonated $\text{H}_2\text{BMI}^{2+}$ cation.

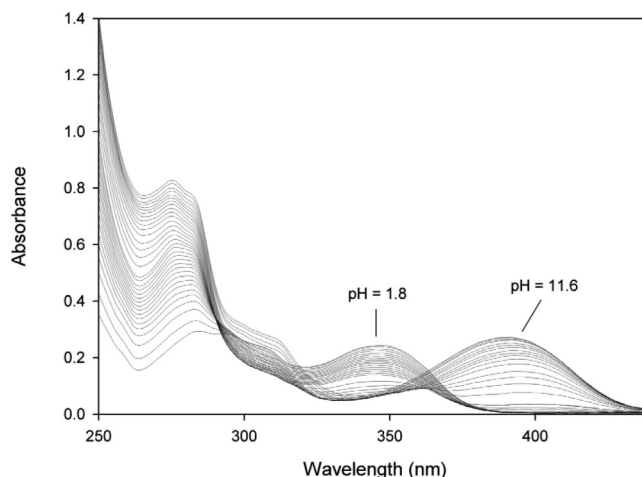


Figure 4. Variable-pH (1.8–11.6) UV–vis spectra of **HBTI** ($[\text{HBTI}] = 0.024 \text{ mM}$, 37°C , $I = 0.10 \text{ M NaCl}$).

On the basis of literature data, the lower pK_a value (3.65) corresponds to deprotonation of the anilinium cation and the higher one (7.44) to that of the protonated imidazole ring.⁶⁶ The first deprotonation step is accompanied by the hypsochromic shift of the low-energy absorption band, while the second one only involves minor changes. The pK_a values found for **HBXI**, **HBTI**, and **BMI** (shown in Table 3) are consistent with previously reported data.⁶⁷ For comparison, the acidity constants of **HCQ** were also determined under the same experimental conditions (Table 3 and Figure S4 in the Supporting Information).

Solution speciation diagrams were calculated using the acidity constants given in Table 3 and are shown in Figure 5. In view of their potential application, it should be noted that the species present at physiological pH ($\text{pH} \approx 7.4$) are different for the three ligands: **HBTI** and **HBXI** are essentially present as neutral molecules (as is **HCQ**), while for the **BMI** ligand at the same pH, the corresponding monoprotonated and totally deprotonated species coexist in solution.

Synthesis and Characterization of Metal Complexes ML_2 [$M = \text{Zn(II)}, \text{Cu(II)}$; $L = \text{BXI}, \text{BTI}, \text{BMI}$]. The **Cu(II)** and **Zn(II)** complexes were readily prepared by mixing the metal chloride salt and the corresponding ligand. In all of the reactions, the solid complex that separated out from the solution as either a brown [**Cu(II)**] or yellow [**Zn(II)**] powder did not afford good quality single crystals, and the ML_2 complex was the only

(66) Martell A. E.; Smith, R. M. *Critical Stability Constants*; Plenum: New York, 1974–1989; Vol. 1–6.

(67) Ulkuseven, B.; Kizilcikli, I.; Tavman, A.; Akkurt, B. *Rev. Inorg. Chem.* **2001**, *21*, 369–379.

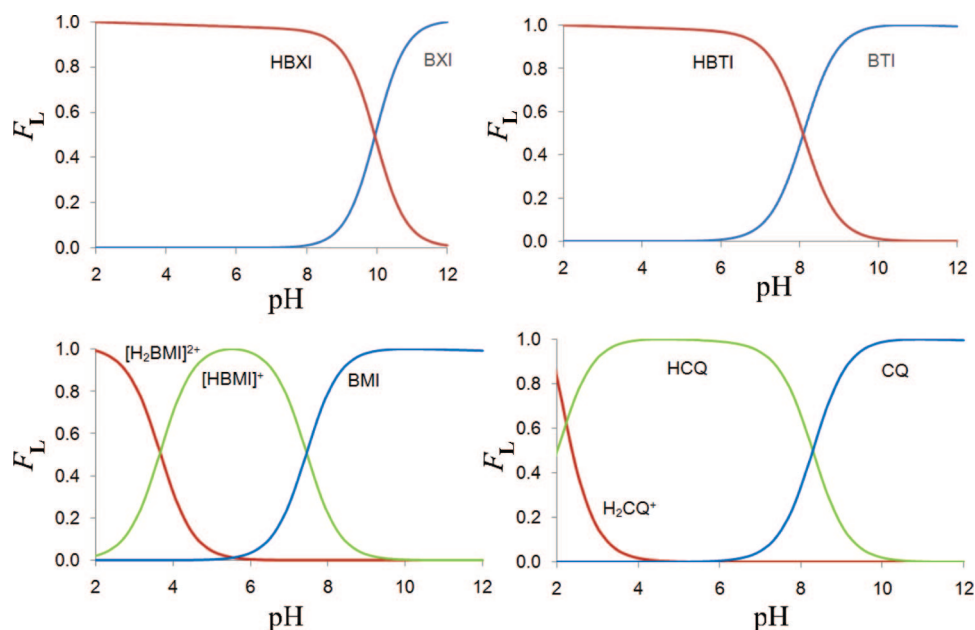


Figure 5. Solution speciation diagrams for **HBXI**, **HBTI**, **BMI**, and **HCQ**. F_L is the fraction of compound with given protonation. Total concentrations: $[\text{HBXI}] = [\text{HBTI}] = [\text{BMI}] = 0.024 \text{ mM}$; $[\text{HCQ}] = 0.12 \text{ mM}$.

species obtained at either 1:2 or 1:1 metal-to-ligand molar ratio. CI-MS measurements on ZnL_2 ($\text{L} = \text{BXI}$, **BTI**) samples were inconclusive with respect to the nuclearity of these species in the solid phase. With closely related ligands, X-ray structures of either mononuclear⁶⁸ or dinuclear⁶⁹ complexes have been reported, involving tetrahedral or distorted trigonal bipyramidal geometry, respectively, around the zinc atom. However, the solution equilibria studies described below are fully consistent with the exclusive formation of mononuclear species with ZnL and ZnL_2 ($\text{L} = \text{BXI}$, **BTI**) stoichiometries. Unlike ZnL_2 ($\text{L} = \text{BXI}$, **BTI**), mass measurements on the zinc complex of the neutral **BMI** ligand, $[\text{Zn}(\text{BMI})_2]\text{Cl}_2$, indicated that it is mononuclear. As regards the copper complexes, the EPR studies described below, mass measurements, and literature data^{68,70} are consistent with mononuclear CuL_2 species for the three ligands $\text{L} = \text{BXI}$, **BTI**, and **BMI**.

Characterization of Cu(II) Complexes by EPR Spectra. The X-band EPR spectra of the Cu(II) complexes $[\text{Cu}(\text{BXI})_2]$, $[\text{Cu}(\text{BTI})_2]$, and $[\text{Cu}(\text{BMI})_2]^{2+}$ in frozen solution (150 K, 1:1 dichloromethane/toluene for $[\text{Cu}(\text{BXI})_2]$ and $[\text{Cu}(\text{BTI})_2]$ and 1:1 ethanol/methanol for $[\text{Cu}(\text{BMI})_2]^{2+}$) show a similar pattern (Figure 6). The spectra show^{63,65} Cu hyperfine splitting in the g_{zz} region: three of the four metal hyperfine lines are observed, and the fourth is partially hidden in the $g_{xx,yy}$ region. The spectra are basically axial in character: there are two very similar g -factor values (g_{xx} and $g_{yy} \approx 2.05$), whereas $g_{zz} \approx 2.25$ (see Table 4). The value of the metal hyperfine coupling constant, A_{zz} , is close to that observed for Cu(II) in an essentially planar environment.⁷¹ The magnitude of A_{zz} and g_{zz} are dependent,

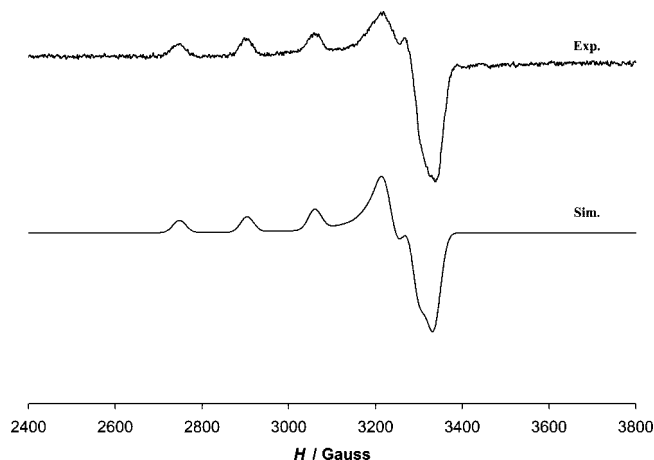


Figure 6. Frozen-solution EPR spectrum of compound $[\text{Cu}(\text{BTI})_2]$ in 1:1 dichloromethane/toluene ($T = 150 \text{ K}$) along with a simulated spectrum.

Table 4. Spin Hamiltonian Parameters Obtained by Simulation of the Frozen-Solution EPR Spectra of Cu(II) Complexes ($T = 150 \text{ K}$) and the f Factor^a

compound	g_{zz}	g_{yy}	g_{xx}	$A_{zz} \text{ (G)}$	$A_{yy} \text{ (G)}$	$A_{xx} \text{ (G)}$	$f \text{ (cm)}^b$
$[\text{Cu}(\text{BXI})_2]$	2.253	2.080	2.045	156	20	20	155
$[\text{Cu}(\text{BTI})_2]$	2.252	2.070	2.040	165	20	10	146
$[\text{Cu}(\text{BMI})_2]^{2+}$	2.240	2.060	2.020	160	10	10	150

^a Solvents: 1:1 dichloromethane/toluene for $[\text{Cu}(\text{BXI})_2]$ and $[\text{Cu}(\text{BTI})_2]$ and 1:1 ethanol/methanol for $[\text{Cu}(\text{BMI})_2]^{2+}$. ^b $f = g_{zz}/A_{zz}$; $A(\text{cm}^{-1}) = 0.46686451 \times 10^{-4} g_{\text{e}} A(\text{G})$.

among other things, on the nature of the ligands bound to Cu(II), which can be used to assign the structure. The tendency of A_{zz} to decrease with increasing g_{zz} is an indicator for the increase in the distortion from square-planar to tetrahedral geometry in the coordination sphere of Cu. In order to quantify the degree of distortion of the Cu(II) complexes, the factor $f = g_{zz}/A_{zz}$ was obtained from the EPR spectra. For square-planar complexes, f -factor values range from 105 to 135 cm .^{72,73} For the investigated complexes, the g_{zz}/A_{zz} quotients are $\sim 150 \text{ cm}$ (Table

(68) Benisvy, L.; Bill, E.; Blake, A. J.; Collison, D.; Davies, E. S.; Garner, C. D.; McArdle, G.; McInnes, E. J. L.; McMaster, J.; Ross, S. H. K.; Wilson, C. *Dalton Trans.* **2006**, 258–267.

(69) Yu, G.; Yin, S.; Liu, Y.; Shuai, Z.; Zhu, D. *J. Am. Chem. Soc.* **2003**, *125*, 14816–14824.

(70) Benisvy, L.; Blake, A. J.; Davies, E. S.; Garner, C. D.; McMaster, J.; Wilson, C.; Collison, D.; McInnes, E. J. L.; Whittaker, G. *Chem. Commun.* **2001**, 1824–1825.

(71) Mabbs, F. E. D. C. *Electron Paramagnetic Resonance of d-Transition Metal Complexes*; Elsevier: Amsterdam, 1992.

4), so there exists some degree of tetrahedral distortion. These results are close to others observed for Cu(II) complexes with similar ligands.^{68,70}

Three-Dimensional Structure of ML₂ Complexes by DFT Calculations. As the heterocyclic five-membered rings in the **HBXI**, **HBTI**, and **BMI** compounds contain two donor atoms suitable for binding Cu(II) and Zn(II) ions, we used DFT calculations to investigate the two possible chelating modes for each ligand: for **HBXI**, N/O–C₆H₃I or O/O–C₆H₃I; for **HBTI**, N/O–C₆H₃I or S/O–C₆H₃I; and for **BMI**, N(sp²)/H₂N–C₆H₃I or NH/H₂N–C₆H₃I (Figure 3). For each system, only the mononuclear complexes were considered, since no other nuclearities were observed in solution. On the basis of the DFT calculations, it can be concluded that for **HBXI** and **HBTI**, the two metal cations have preference for coordination through the N atom of the benzoxazole or benzothiazole fragment, as the O/O–C₆H₃I and S/O–C₆H₃I coordinations lie ~50–70 kcal mol^{–1} above that involving the N(sp²) atom of the heterocyclic ring. For **BMI**, the preferred coordination is always through the N(sp²) atom of the benzimidazole moiety, which is completed with the aniline NH₂ group.

The B3LYP-optimized geometries for the most stable complexes formed between the Cu(II) and Zn(II) ions and the selected ligands are shown in Figure 7. As a general trend, it can be observed that the Cu(II)-containing complexes adopt distorted square-planar geometries, in agreement with the EPR experiments, whereas those enclosing Zn(II) present tetrahedral coordination. Both coordination geometries are fully consistent with the preferences of Cu(II) and Zn(II) ions in complexes with a coordination number of 4. Remarkably, coordination to the metal cation induces changes in the ligand planarity, i.e., on the torsional angle between the two ligand moieties. Comparisons of the DFT results obtained for the uncoordinated and bound **HBXI**, **HBTI**, and **BMI** ligands show that the largest deviation occurs for **BMI**, where the N–C–C torsional angle increases from 5 to 27 or 28° for the Cu²⁺ or Zn²⁺ complexes, respectively. This is not surprising, considering that the energy barrier associated with the rotation around the central C–C bond in **BMI** is the lowest of the three ligands (values not shown) and that this distortion is required for an optimal interaction with the metal ion. For the anionic **BXI** and **BTI** ligands, the deviation from planarity upon coordination is much smaller, ~1° when either of them binds to Zn(II) and 3 and 12°, respectively, when they interact with Cu(II). The larger distortion in the latter complexes can be attributed to the square-planar coordination geometry around Cu(II), which involves larger ligand–ligand repulsions than in the tetrahedral coordination adopted by Zn(II). Moreover, it can be observed that the metal–ligand distances are always shorter in the Cu(II) complexes than in the Zn(II) complexes, in accordance with the larger Pauli repulsion between the metal cation and the ligand in the case of Zn(II). Consistently, chelation to Cu(II) should be more favorable than that to Zn(II) because of an enhanced electrostatic interaction.

Spectrophotometric Determination of the Stability Constants of ML₂. Solution equilibria studies were performed under conditions similar to physiological media (*T* = 310 K, *I* = 0.10 M NaCl). The experimental variable-pH UV–vis curves obtained by titration of solutions containing metal ions and

ligands at different molar ratios closely fit those simulated by assuming the existence of ML and ML₂ species with the stability constants shown in Table 3. The p*K*_a values for the ligands as well as the hydrolysis constants for the free Cu(II) and Zn(II) ions were taken into account in the calculations.⁷⁴ No metal hydrolysis species of significance were present in any of the systems studied. On the basis of the calculated constants, solution speciation diagrams for Cu(II) and Zn(II) with **HBXI**, **HBTI**, and **BMI** at metal-to-ligand molar ratios of 1:2 are depicted in Figure 8.

The overall stability constants (log β) calculated for the ML₂ complexes formed by the **HBXI**, **HBTI**, and **BMI** ligands (Table 3) show that they have a stronger ability to bind copper than zinc, consistent with the reported data for related compounds. For a particular metal ion, the binding affinity follows the order **HBXI** > HCQ > **HBTI** > **BMI**, which is consistent with the general rule for a series of similar ligands that the binding constants increase with increasing ligand basicity (Table 3). From the speciation diagrams it is evident that within the pH range examined, the stoichiometries of the existing species are identical for both Zn(II) and Cu(II). Moreover, the concentration of free Cu(II) or Zn(II) ions above pH 4 with either ligand is negligible. These diagrams also allow calculation of the concentration of each species under specific experimental conditions. Thus, the concentrations of unchelated Cu(II) at pH 6.6 and Zn(II) at pH 7.4 (given as pM = –log[M_{free}]) for solutions containing 25 μM metal and 50 μM ligand are given in Table 3. The pM values not only reflect the metal binding affinities of the **HBXI**, **HBTI**, and **BMI** ligands at a specific pH value but also allow predictions of their abilities to sequester Zn(II) and Cu(II) ions bound to Aβ peptide. Considering that the different values reported for the binding constants are in the nanomolar range for Cu(II)^{75–78} and in the micromolar range for Zn(II),^{76,79} we could conclude that **HBXI** and **HBTI** are expected to sequester these metal ions from soluble forms of Aβ. This hypothesis is supported by the Aβ aggregation inhibition studies described in the next section.

Inhibition of Aβ Aggregation by HBXI, HBTI, and BMI in the Presence or Absence of Metals. The capacity of the iodinated compounds **HBXI**, **HBTI**, and **BMI** to interfere with amyloid fibril formation by the Aβ peptide was investigated in order to assess whether they are able to add an aggregation inhibition ability to their metal chelating features, intercalation properties, and putative radioisotopic traceability. Since ThT fluoresces over the same wavelength range as the tested compounds, rendering it unable to quantify the presence of amyloid fibrils in compound-treated samples, a modification of a previously published turbidimetric assay⁴ was used in this case. On the basis of previous reports, the presence of metal ions such as Zn²⁺ and Cu²⁺ promotes the aggregation of Aβ, thus contributing to the pathogenesis of AD.¹⁴

Consequently, we performed the turbidimetry assays in the absence and presence of Zn(II) and Cu(II) (Figure 9a). The

(72) Bhalla, R.; Helliwell, M.; Garner, C. D. *Inorg. Chem.* **1997**, *36*, 2944–2949.

(73) Yokoi, H.; Addison, A. W. *Inorg. Chem.* **1977**, *16*, 1341–1349.

(74) Baes, C. F., Jr.; Mesmer, R. E. *The Hydrolysis of Cations*; R. E. Krieger Publishing Co.: Malabar, FL, 1986.

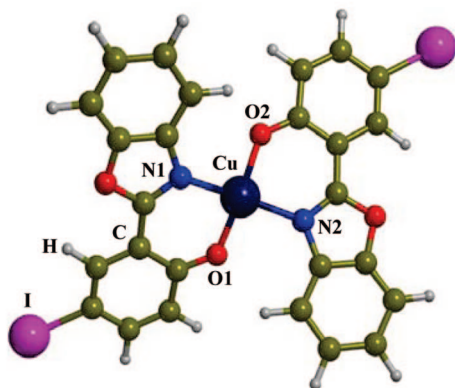
(75) Hatcher, L. Q.; Hong, L.; Bush, W. D.; Carducci, T.; Simon, J. D. *J. Phys. Chem. B* **2008**, *112*, 8160–8164.

(76) Tougu, V.; Karafin, A.; Palumaa, P. *J. Neurochem.* **2008**, *104*, 1249–1259.

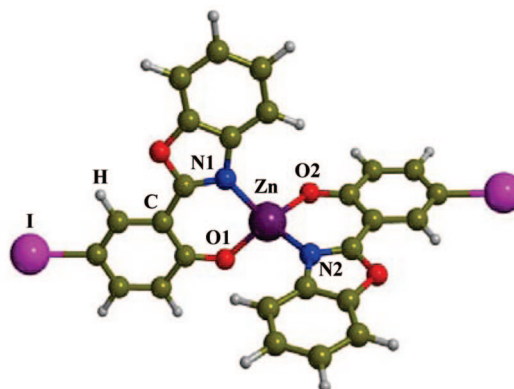
(77) Kowalik-Jankowska, T.; Ruta, M.; Wisniewska, K.; Lankiewicz, L. *J. Inorg. Biochem.* **2003**, *95*, 270–282.

(78) Karr, J. W.; Szalai, V. A. *Biochemistry* **2008**, *47*, 5006–5016.

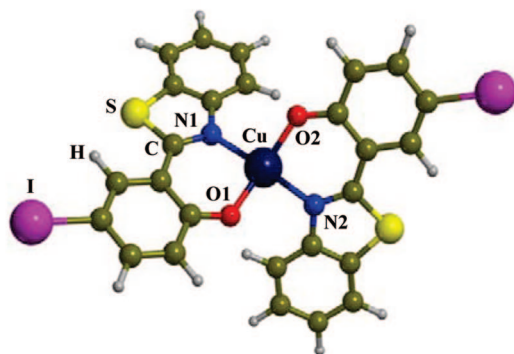
(79) Talmard, C.; Bouzan, A.; Faller, P. *Biochemistry* **2007**, *46*, 13658–13666.

[Cu(BXI)₂]

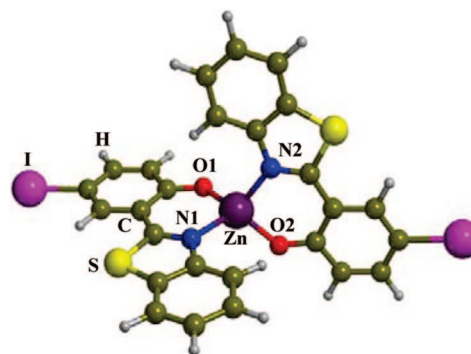
Cu-O1 = 1.917; Cu-O2 = 1.917; Cu-N1 = 2.004; Cu-N2 = 2.004;
O1CuN1 = 91.6; N1CuO2 = 93.3; O2CuN2 = 91.6; N2CuO1 = 93.3;
O1N1N2O2 = 133.4; N1CCC = 3.1

[Zn(BXI)₂]

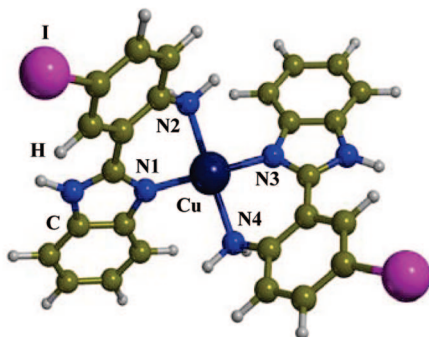
Zn-O1 = 1.929; Zn-O2 = 1.929; Zn-N1 = 2.036; Zn-N2 = 2.036;
O1ZnN1 = 93.5; N1ZnO2 = 113.5; O2ZnN2 = 93.5; N2ZnO1 = 113.5;
O1N1N2O2 = 82.7; N1CCC = -1.5

[Cu(BTI)₂]

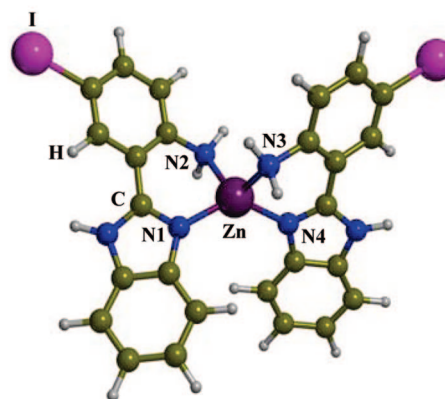
Cu-O1 = 1.904; Cu-O2 = 1.904; Cu-N1 = 2.024; Cu-N2 = 2.024;
O1CuN1 = 91.8; N1CuO2 = 95.0; O2CuN2 = 91.8; N2CuO1 = 95.0;
O1N1N2O2 = -125.1; N1CCC = -12.5

[Zn(BTI)₂]

Zn-O1 = 1.917; Zn-O2 = 1.917; Zn-N1 = 2.049; Zn-N2 = 2.049;
O1ZnN1 = 93.9; N1ZnO2 = 114.5; O2ZnN2 = 93.9; N2ZnO1 = 114.5;
O1N1N2O2 = 73.1; N1CCC = 1.2

[Cu(BMI)₂]

Cu-N1 = 1.976; Cu-N2 = 2.095; Cu-N3 = 1.978; Cu-N4 = 2.095;
N1CuN2 = 85.3; N2CuN3 = 95.9; N3CuN4 = 85.3; N4CuN1 = 95.9;
N1N2N4N3 = 155.3; N1CCC = 26.9

[Zn(BMI)₂]

Zn-N1 = 1.984; Zn-N2 = 2.112; Zn-N3 = 2.112; Zn-N4 = 1.984;
N1ZnN2 = 90.9; N2ZnN3 = 116.4; N3ZnN4 = 90.9; N4ZnN1 = 129.7;
N1N2N4N3 = -73.3; N1CCC = 28.3

Figure 7. Selected bond distances (Å) and angles (deg) in the B3LYP-optimized [ML₂] (L = BXI, BTI, BMI) complexes.

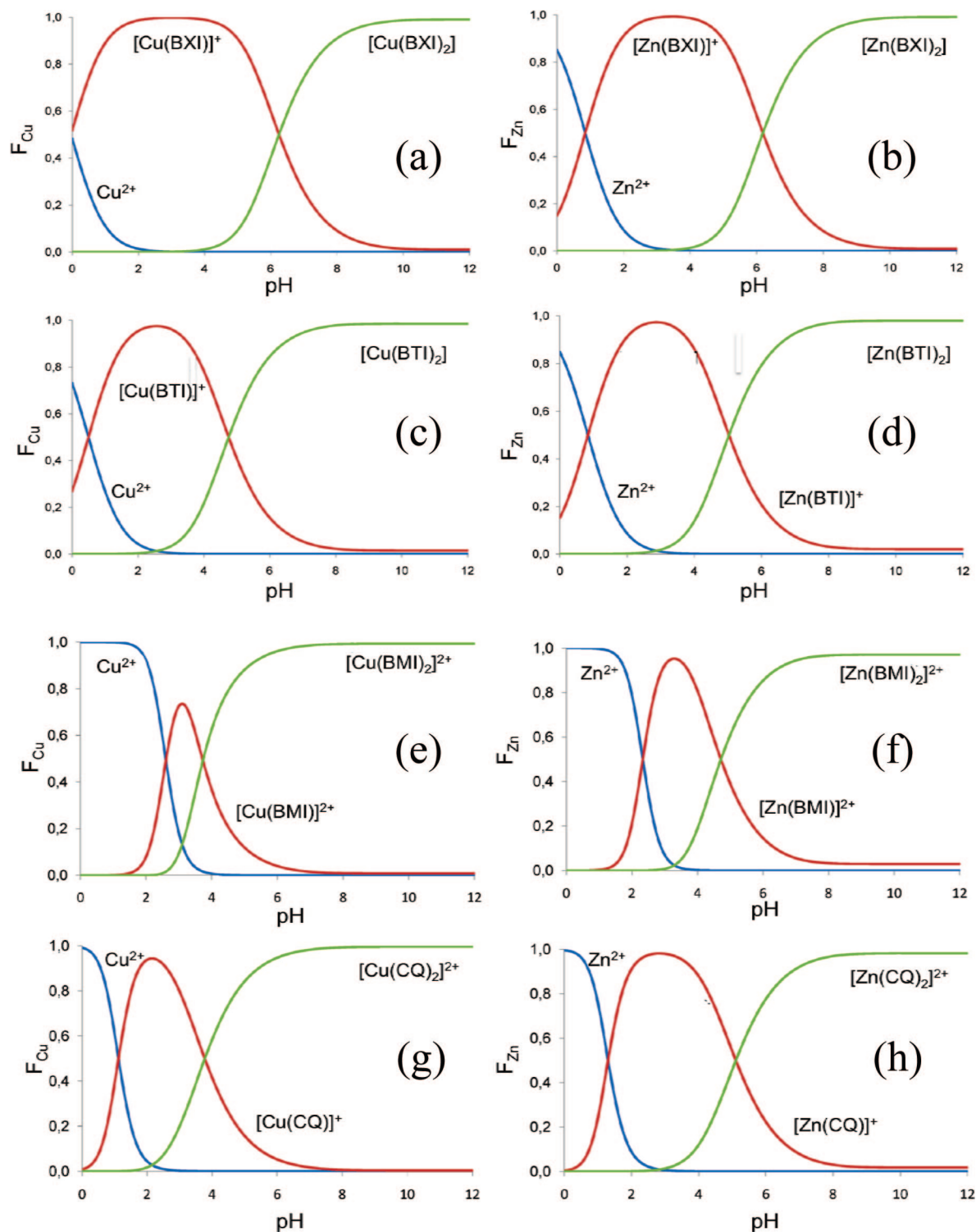


Figure 8. Solution speciation diagrams for (a) **HBXI** and Cu(II), (b) **HBXI** and Zn(II), (c) **HBTI** and Cu(II), (d) **HBTI** and Zn(II), (e) **BMI** and Cu(II), (f) **BMI** and Zn(II), (g) **HCQ** and Cu(II), and (h) **HCQ** and Zn(II). Conditions: $[M(II)]/[ligand] = 1:2$, $[M(II)]_{tot} = 25 \mu M$.

results show that their presence in solution increases $A\beta_{1-40}$ aggregation by a factor of ~ 3 compared with that obtained from freshly dissolved $A\beta_{1-40}$ after overnight incubation. Within this context, depletion of the cations from solution by complexation with a reference chelator such as EDTA prevents most of the ion-promoted aggregation effect. The three compounds studied in this work have little influence on the aggregation of $A\beta_{1-40}$ in the absence of metals, but they clearly decrease fibril buildup

in the presence of Cu^{2+} . This effect follows the order **HBXI** > **HBTI** > **BMI**, which parallels the concentration of free Cu(II) ions as deduced by the pCu values given in Table 3. Remarkably, inhibition of Zn^{2+} -promoted aggregation is only significant for **HBTI**, whose behavior compares well with that for **HCQ**, the two compounds having similar abilities to reduce metal-induced aggregation. In regard to intercalating compounds devoid of chelating properties, ThT did not have any effect on

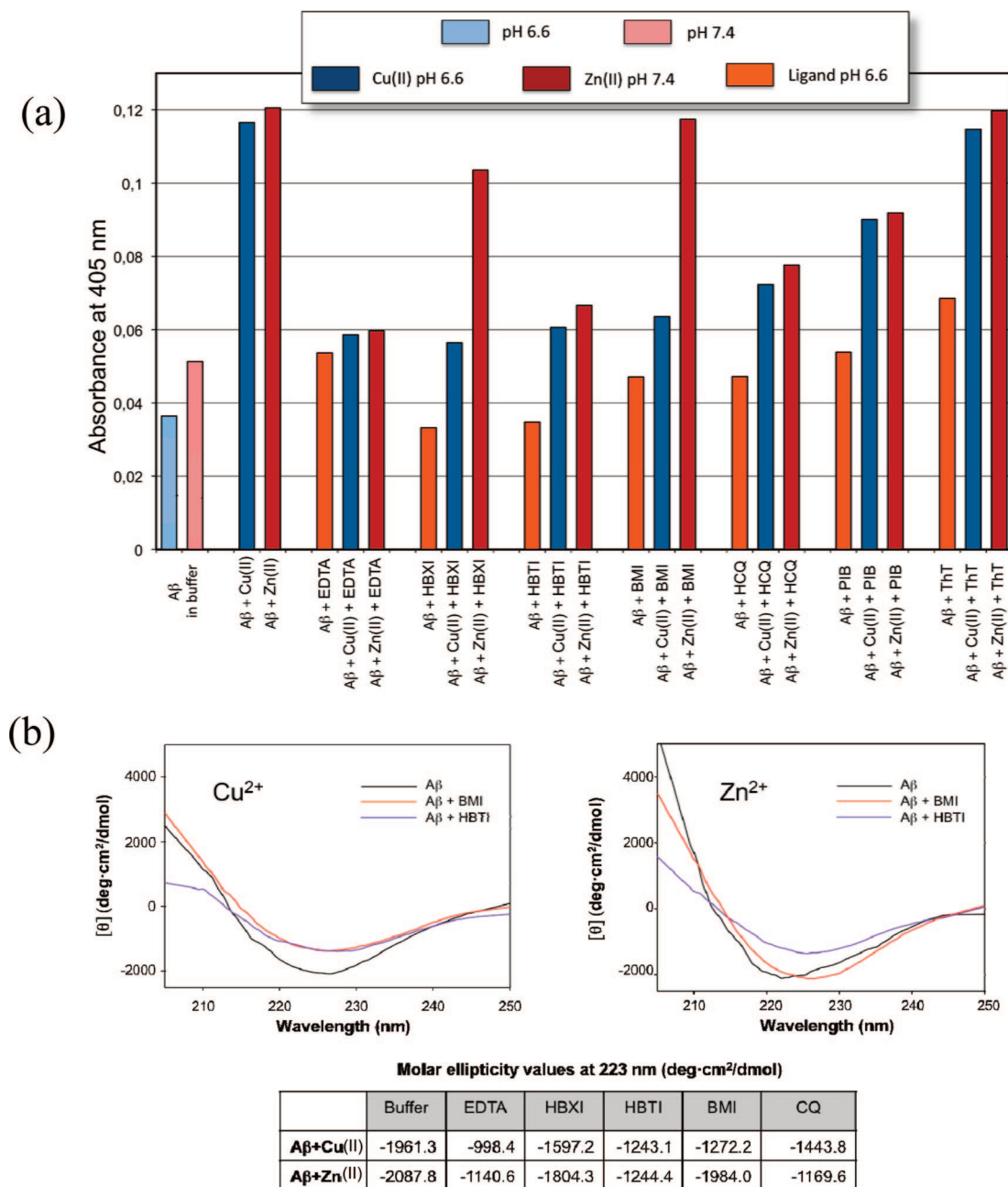


Figure 9. (a) Turbidimetry assays to follow the aggregation inhibition of $A\beta_{1-40}$. Absorbance was measured at 405 nm, and the values indicate the means of two different assays in which every sample was measured four times. The compounds analyzed were compared with EDTA and CQ as chelator references and with PIB and ThT as amyloid markers. (b) Far-UV CD spectra of 25 μ M $A\beta_{1-40}$ in the presence of Cu(II) or Zn(II) and the indicated compounds. The table shows the intensities (in molar ellipticity units) of the major negative band at 223 nm in the $A\beta_{1-40}$ spectra in the presence of the indicated metals and compounds.

aggregation, whereas PIB appeared to be able to weakly reduce aggregation through an as yet unknown mechanism.

To obtain further evidence to support the observations deduced from the turbidimetry assays, the secondary-structure content of $A\beta_{1-40}$ peptide in the presence of Cu^{2+} , Zn^{2+} , and the compounds here studied was analyzed by CD (Figure 9b). The CD spectra of $A\beta_{1-40}$ in the presence of Cu(II) and Zn(II) exhibit a negative band at 223–225 nm characteristic of $A\beta_{1-40}$ aggregated in protofibrillar/fibrillar conformations⁸⁰ and contributed mainly by β -sheet secondary structure. Overall, the molar ellipticity values given in Figure 9b show that the CD results correlate well with those obtained from the turbidimetry assays. Significantly, according to both experiments, **HBTI** is able to

reduce $A\beta_{1-40}$ peptide aggregation in the presence of Cu(II) and Zn(II), whereas **HBXI** and **BMI** are only efficient for Cu(II)-induced aggregation.

The observation of a differential effect on Cu^{2+} - and Zn^{2+} -promoted aggregation might suggest that the compounds are not acting as unspecific chelators but rather recognize a subpopulation of Cu^{2+} cations involved in the self-assembly of the peptide and that their amyloid binding properties might facilitate this action. Indeed, it has been reported that different mechanisms lie behind Zn^{2+} - and Cu^{2+} -induced aggregation.

(80) Huang, T. H.; Yang, D. S.; Plaskos, N. P.; Go, S.; Yip, C. M.; Fraser, P. E.; Chakrabarty, A. *J. Mol. Biol.* **2000**, 297, 73–87.

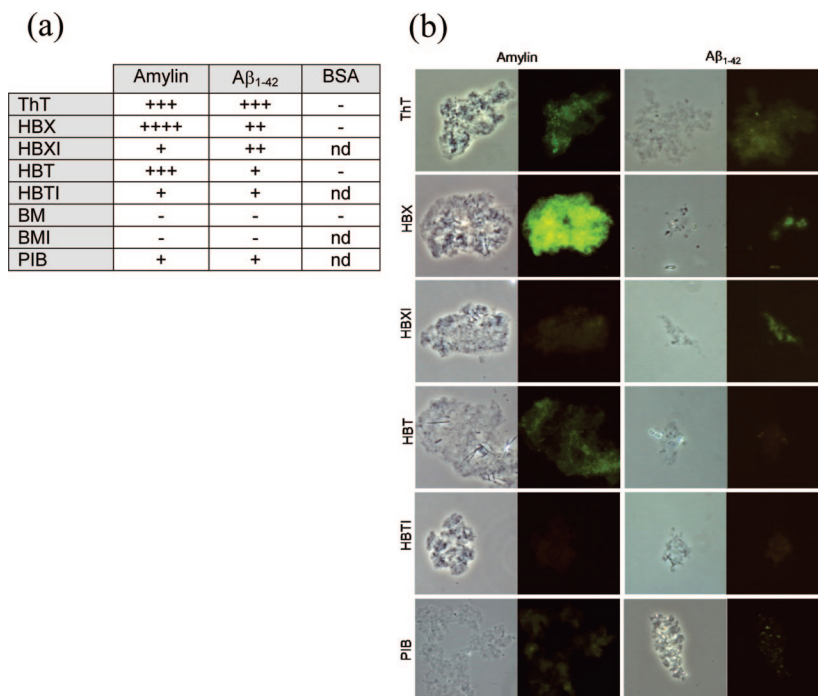


Figure 10. (a) Table of the relative fluorescences of fibrils treated with the different compounds. The fibrous material was visualized under a fluorescence microscope. The qualitative intensity measure ranges from ++++ (very intense) to – (no fluorescence); nd = not determined. (b) Visualization of fibril staining with selected compounds. Images are shown both for amylin (IAPP_{10–29} fragment) and A β_{1-42} pre-grown fibrils. Magnifications of 40 and 100 \times were used for amylin and for A β_{1-42} , respectively. Columns 1 and 3 show phase-contrast microscopy images to account for the presence of fibrils, and columns 2 and 4 show fluorescence microscopy images. Staining with ThT is shown as a positive control. Negative binding controls with BSA, indicating the absence of aggregates or fluorescence, are not shown.

In the case of copper, changes in peptide conformation are modulated by subtle variations in the acidic conditions.⁸¹ Besides, while the Cu(II) ion forms a stable, soluble 1:1 complex with A β , the interaction with Zn(II) is more complicated and involves different complex-formation steps.⁷⁶ In addition to direct effects on A β aggregation, Cu²⁺ catalyzes the generation of reactive oxygen species in the brain,^{14,82} further contributing to neurodegeneration. Disruption of these aberrant metal–peptide interactions via chelation therapy could thus be considered as a promising therapeutic strategy for combating this disease.

Intercalation Properties of Compounds HBX, HBT, and BM and Their Iodinated Derivatives into Amyloid Fibrils. Binding to Different Protein Amyloids. Amyloid fibrils may arise from the aggregation of a wide range of different proteins. Two disease-related polypeptides were used to test the intercalation properties of the compounds under assay: A β_{1-42} and IAPP, a 37-residue hormone that cosecretes with insulin and builds up amyloid deposits in the pancreas in type-II diabetes.^{83,84} The use of diagnostic dyes to detect amyloid is based on the spectral changes (increase in absorbance or fluorescence emission and shift of their maxima) that molecules like ThT or CR exhibit after binding to the ordered crossed β -sheet structure of amyloid aggregates.^{12,85} As the compounds analyzed herein are them-

selves fluorescent, initial tests were conducted to check whether the presence of amyloid fibrils specifically affects their emission spectra upon excitation at their respective excitation maxima. While significant spectral changes were detected for compounds **HBT** and **HBX**, suggesting a specific interaction with the fibrils, neither a shift in the absorption maximum nor an increase in fluorescence was observed for **BM** (see Figure S5 in the Supporting Information). These results indicate that **HBX** and **HBT** could behave as potential markers for the presence of amyloid fibrils. In contrast, the low absorption of compound **BM** at the wavelengths where fluorescence microscopy measurements are made (see below) advises against its use for this purpose.

As fluorescence microscopy is a complementary method for assessing the interaction with amyloid fibrils, binding tests were conducted on both A β_{1-42} and IAPP_{10–29} pre-grown fibrils for all of the compounds described herein and also for ThT and PIB. While both of the latter two compounds have shown their suitability to behave as a fibril control,⁸⁶ PIB is already being used clinically.^{87,88} The results of our experimental setup are shown in Figure 10a in terms of relative intensity. Selected images in which areas rich in fibrous material are visible and give a bright green-yellow fluorescence of variable degree are shown in Figure 10b for fibrils treated with compounds **HBT** and **HBX** and their iodinated derivatives. The differences observed in the fluorescence emission of these compounds indicate a certain degree of binding specificity, which is probably related to subtle differences in the conformation of the fibril

(81) Atwood, C. S.; Moir, R. D.; Huang, X.; Scarpa, R. C.; Bacarra, N. M. E.; Romano, D. M.; Hartshorn, M. A.; Tanzi, R. E.; Bush, A. I. *J. Biol. Chem.* **1998**, 273, 12817–12826.

(82) Meloni, G.; Faller, P.; Vasak, M. *J. Biol. Chem.* **2007**, 282, 16068–16078.

(83) Clark, A.; Cooper, G. J.; Lewis, C. E.; Morris, J. F.; Willis, A. C.; Reid, K. B.; Turner, R. C. *Lancet* **1987**, 2, 231–234.

(84) Goldsbury, C.; Goldie, K.; Pellaud, J.; Seelig, J.; Frey, P.; Muller, S. A.; Kistler, J.; Cooper, G. J.; Aebi, U. *J. Struct. Biol.* **2000**, 130, 352–362.

(85) LeVine, H., III *Amyloid* **1995**, 2, 1–6.

(86) Fodero-Tavoletti, M. T.; et al. *J. Neurosci.* **2007**, 27, 10365–10371.

(87) Ziolkowski, S. K.; Weissfeld, L. A.; Klunk, W. E.; Mathis, C. A.; Hoge, J. A.; Lopresti, B. J.; DeKosky, S. T.; Price, J. C. *NeuroImage* **2006**, 33, 94–102.

(88) Nordberg, A. *Neuropsychologia* **2008**, 46, 1636–1641.

peptide backbones. PIB gives a weaker signal than **HBT** or **HBX**, indicating that, at least in regard to fluorescence staining of mature fibrils, these compounds compare favorably with one of the few molecules used in clinical trials. Remarkably, fibrils treated with compound **HBX** display a stronger fluorescence signal than those treated with the commonly used ThT dye. The intercalation properties observed for **HBXI** and **HBTI** through fluorescence measurements show that these compounds might be especially suitable for radioisotopic detection of $A\beta_{1-42}$ deposits in the human brain.

Compounds closely related to **HBXI**, **HBTI**, and **BMI** are widely known for their photoluminescence properties.⁸⁹ All three ligands are characterized by an intramolecular hydrogen bond between a proton donor in the phenyl moiety ($-\text{OH}$ in **HBXI** or **HBTI** or $-\text{NH}_2$ in **BMI**) and the $-\text{N}=\text{}$ proton acceptor in the benzoxazole, benzothiazole, or benzimidazole moiety (Figure 3). When these molecules are photoexcited, there is an electronic charge redistribution that enhances the acidity of the proton donor and the basicity of the proton acceptor, giving rise to a fast elementary process described as an excited-state intramolecular proton-transfer reaction. This isomerization between the normal form (N) and the proton-transferred tautomeric form (T) in the excited state, $\text{N}^* \rightarrow \text{T}^*$, is shown by a large Stokes shift in the emission spectra and has been the subject of several experimental and theoretical studies.^{90–95} These have shown that the dynamics of this reaction is determined by the shape of the potential energy surface. In order to understand the different behavior of **HBXI**, **HBTI**, and **BMI**, we therefore used the TDDFT formalism to compute the first singlet excited electronic state for each molecule. Figure S6 in the Supporting Information shows the energy profiles for the intramolecular proton transfer processes in the ground (S_0) and the first excited (S_1) state. As expected, this process is unfavorable in the ground state, the tautomerization reaction energies being 13.0, 11.5, and 19.9 kcal mol⁻¹ for **HBXI**, **HBTI**, and **BMI**, respectively. However, in the first excited state, the reaction becomes much more favorable because of an enhancement of the proton-donor acidity and the proton-acceptor basicity. For **HBXI** and **HBTI**, the excited-state tautomeric form T^* becomes more stable than the excited-state normal form N^* by 4.8 and 5.4 kcal mol⁻¹, respectively, in such a way that the wavelengths of the fluorescence processes from these minima are computed to be 468 and 485 nm, respectively. However, for **BMI**, although the proton-transfer reaction is also more favorable in S_1 than in S_0 , the tautomer T^* is less stable than N^* by 1.6 kcal mol⁻¹. This is not surprising, considering that the $-\text{NH}_2$ group is less acidic than $-\text{OH}$. In this case, fluorescence is therefore expected to arise mainly from N^* , with a computed wavelength of 396 nm. These results are strongly consistent with the experimental fluorescence spectra of **HBXI**, **HBTI**, and **BMI** (data not shown), for which the maxima of the most intense fluorescence

bands appear at ~ 490 , 520, and 415 nm, respectively. In other words, **HBXI** and **HBTI** present a large Stokes-shifted intense band, whereas **BMI** shows normal fluorescence. The differences between the theoretical and experimental results are due to the limitations of the method and to the fact that solvent interactions are not taken into account in the calculations. Nevertheless, the trends observed in the experimental fluorescence spectra appear to be properly reproduced by the calculations. Moreover, since the long-wavelength emission band is very sensitive to hydrogen-bonding interactions and the polarity of the solvent, it is not surprising that **HBXI** and **HBTI** show larger fluorescence changes upon interaction with the fibrils.

Summary

The incorporation of chelating properties into well-known intercalation compounds has been shown to be successful in the design of new multifunctional agents for application in Alzheimer's disease. This strategy, which has very few precedents, defines new alternatives for developing the next generation of agents for Alzheimer's therapy. In this study, the thioflavin-T molecule, a traditional dye widely used as marker to examine in vitro tissues for amyloid deposits, was used as a reference to afford a molecular framework, **M1**, that integrates amyloid binding and metal chelating properties.

In order to reduce costs, commercial compounds enclosing **M1** were identified using in silico tools and virtual screening methods. The latter ensure that the selected compounds fulfill the main therapeutic requirements: (a) antioxidant properties, (b) susceptibility to iodination for their use as imaging agents, (c) suitability for crossing the blood–brain barrier, and (d) pharmacokinetic properties as defined by Lipinski's rules. Within this context, the commercially available compounds **HBX**, **HBT**, and **BM** were iodinated and the corresponding derivatives **HBXI**, **HBTI**, and **BMI** characterized by X-ray diffraction and DFT calculations.

The coordination features of the synthesized ML_2 [$\text{M} = \text{Cu(II)}$, Zn(II) ; $\text{L} = \text{BXI}$, BTI , BMI] complexes were also analyzed by DFT methods and, in the case of Cu(II) , by EPR spectroscopy. Solution studies on the binding properties of these compounds toward Cu(II) and Zn(II) by UV–vis pH titrations indicate that the metal chelating abilities of **HBXI** and **HBTI** are comparable to that of clioquinol, whereas that of **BMI** is somewhat smaller. Moreover, the calculated stability constants for the ML_2 complexes evidence that **HBXI**, **HBTI**, and **BMI** can be efficient chelators for sequestering the Cu(II) and Zn(II) metal ions that are present in soluble $A\beta$ peptide forms, and this result was also confirmed by the $A\beta$ aggregation turbidity assays, especially in the case of Cu(II) .

Finally, the fluorescence measurements on **HBX**, **HBT**, **BM**, and the corresponding iodinated derivatives show that the emission spectra of **HBX** and **HBT** as well as those of the iodide species significantly change in the presence of amyloid fibrils, which confirms the intercalation properties of these ligands and their potential use for radioisotopic detection of $A\beta_{1-42}$ deposits in the human brain.

Overall, these preliminary findings are evidence of the potential of thioflavin-based intercalation compounds with integrated metal chelating properties as candidates for targeting Alzheimer's amyloidogenesis and warrant further investigations.

Acknowledgment. The authors gratefully acknowledge financial support from MCYT and DURSI through the EET2002-05157-C05-03, CTQ2004-01462, CTQ2005-08797-C02-02/BQU, BIO2007-

- (89) Tong, Y.-P.; Zheng, S.-L.; Chen, X.-M. *Inorg. Chem.* **2005**, *44*, 4270–4275.
- (90) Ríos Vázquez, S.; Ríos Rodríguez, M. C.; Mosquera, M.; Rodríguez-Prieto, F. *J. Phys. Chem. A* **2008**, *112*, 376–387.
- (91) Guallar, V.; Moreno, M.; Lluch, J. M.; Amat-Guerri, F.; Douhal, A. *J. Phys. Chem.* **1996**, *100*, 19789–19794.
- (92) Purkayastha, P.; Chattopadhyay, N. *Phys. Chem. Chem. Phys.* **2000**, *2*, 203–210.
- (93) Santra, S.; Dogra, S. K. *Chem. Phys.* **1998**, *226*, 285–296.
- (94) Santra, S.; Krishnamoorthy, G.; Dogra, S. K. *J. Phys. Chem. A* **2000**, *104*, 476–482.
- (95) Forés, M.; Duran, M.; Solà, M.; Orozco, M.; Luque, F. J. *J. Phys. Chem. A* **1999**, *103*, 4525–4532.
- (96) Jeffrey, G. A.; Lewis, L. *Carbohydr. Res.* **1978**, *60*, 179–182.

68046, SGR2005-00244, SGR2005-00896, and SGR2005-01037 projects and the use of the Catalonia Supercomputer Centre (CESCA). We are grateful to Dr. Jordi Mestres of IMIM (Barcelona, Spain) for his help with chemoinformatic tools, to Dr. Gregori Valencia and Dra. Gemma Arsequell of the IIBB-CSIC (Barcelona, Spain) for interesting discussions on iodination reactions, and to Dr. Emmanuel Gras of CNRS-Université Paul Sabatier UMR 5068 (Toulouse, France) for his generous donation of a sample of PIB.

Supporting Information Available: Complete refs 16, 43, and 86; structures of alternative ligands resulting from the virtual

screening process; crystal and refinement data for **HBXI**, **HBTI**, and **BMI**; variable-pH UV–vis titration data for **HBXI**, **BMI**, and **HCQ**; fluorescence spectra of **HBX**, **HBT**, **BM**, and **ThT** in the presence or absence of fibrils; energy profiles of the intramolecular proton transfer in the ground (S_0) and excited (S_1) states of **HBXI**, **HBTI**, and **BMI**; and X-ray crystallographic data in CIF format for **HBXI**, **HBTI**, and **BMI**. This material is available free of charge via the Internet at <http://pubs.acs.org>.

JA806062G